Polar Radiation Budgets of the NCAR CCM3*,+

BRUCE P. BRIEGLEB

National Center for Atmospheric Research,# Boulder, Colorado

DAVID H. BROMWICH

Polar Meteorology Group, Byrd Polar Research Center, Ohio State University, Columbus, Ohio

(Manuscript received 18 June 1997, in final form 3 November 1997)

ABSTRACT

Present-day Arctic and Antarctic radiation budgets of the National Center for Atmospheric Research Community Climate Model version 3 (CCM3) are presented. The CCM3 simulation is from a prescribed and interannually varying sea surface temperature integration from January 1979 through August 1993. Earth Radiation Budget Experiment (ERBE) data from 1985 through 1989 are used for validation of top-of-atmosphere (TOA) absorbed shortwave radiation (ASR) and outgoing longwave radiation (OLR). Summer ASR in both polar regions is less than the observations by about 20 W m^{-2}. While the annual mean OLR in both polar regions is only 2–3 W m^{-2} less than the ERBE data, the seasonal amplitude in OLR of 40 W m^{-2} is smaller than the observed of 55–60 W m^{-2}. The annual polar TOA radiation balance is smaller than observations by 5–10 W m^{-2}. Compared to selected model and observational surface data, downward shortwave (SW) is too small by 50–70 W m^{-2} and downward longwave (LW) too large by 10–30 W m^{-2}. Surface downward LW in clear atmospheres is too small by 10–20 W m^{-2}. The absence of sea-ice melt ponds results in 10–20 W m^{-2} too much SW absorption during early summer and from 20 to 40 W m^{-2} too little during late summer. Summer cloud covers are reasonably well simulated, but winter low cloud cover is too high by 0.5–0.7 compared to surface cloud observations. Comparison with limited satellite and in situ observations indicates cloud water path (CWP) is too high by about a factor of 2. While cloud particle sizes are approximately in the range of observed values, regional variation between maritime and continental droplet sizes is too strong over coastlines. Despite several improvements in CCM3 radiation physics, the accuracy of polar TOA annual radiation balance is degraded against the ERBE data compared to CCM2. Improvement in CCM3 polar radiation budgets will require improved simulation of CWP, clear sky LW, and sea ice albedo.

1. Introduction

The present issue contains many papers on the National Center for Atmospheric Research (NCAR) Climate System Model (CSM), a comprehensive global climate model consisting of an atmospheric component [Community Climate Model version 3 (CCM3)], an ocean component, a land surface component, and a sea-ice component coupled together with the flux conserving flux coupler. An overview of the NCAR CSM is given by Boville and Gent (1998).

To understand the CSM behavior in century-long control and climate change integrations, as well as to have a basis for further improvements in the component models, it is necessary to assess the uncoupled model simulation of present-day climate. In the uncoupled CCM3 simulation, the ocean is represented by prescribed monthly sea surface temperatures (SSTs) and sea-ice distribution. The uncoupled climate simulation of CCM3 is described in four papers in the present issue: Kiehl et al. (1998a), Kiehl et al. (1998b), Hack et al. (1998), and Hurrell et al. (1998). As noted in Kiehl et al. (1998b), it is important to consider not only the top-of-atmosphere (TOA) radiation budgets, but also the surface radiation budgets, because accurate TOA radiation budgets do not always mean accurate partitioning of radiative heating between atmosphere and surface. Biases in surface radiation budgets have important consequences in coupled climate models such as CSM. In contrast to Kiehl et al. (1998b), who used the NCAR Ocean Model (NCOM) surface-forcing data for model evaluation, we employ other data, since the NCOM data were highly simplified over ice-covered oceans. The present paper is the first part of a two part assessment

* An electronic supplement to this article may be found on the CD-ROM accompanying this issue or at http://www.ametsoc.org/AMS.

+ Contribution 1069 of Byrd Polar Research Center.

The National Center for Atmospheric Research is sponsored by the National Science Foundation.

Corresponding author address: Bruce P. Briegleb, NCAR/CGD, P.O. Box 3000, Boulder, CO 80307-3000.
E-mail: bruceb@ucar.edu

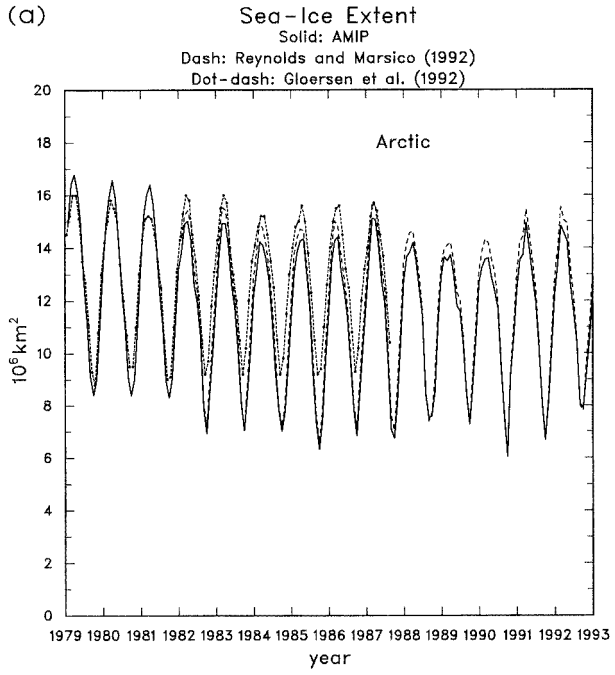

FIG. 1. Monthly mean Arctic (a) and Antarctic (b) sea-ice extent over the period of January 1979–December 1992. The solid line is the extent inferred from the AMIP SSTs; the dashed line (from January 1982–December 1992) is the ice extent inferred from the blended SST data of Reynolds and Marsico (1993); the dot–dashed line (from January 1979–June 1987) is the ice extent based on passive microwave observations from Gloersen et al. (1992).

TABLE 1. Polar cap (70°–90° lat) seasonal and annual TOA ASR, OLR, and annual radiation budget (RDB) CCM3 and ERBE (1985–89) W m^{-2}. Diff column is CCM3 minus ERBE.

	Arctic			Antarctic		
	CCM3	ERBE	Diff	CCM3	ERBE	Diff
Winter		(DJF)			(JJA)	
ASR	1.5	1.2	+0.3	1.0	0.8	+0.2
OLR	172	165	+7	141	135	+6
Summer		(JJA)			(DJF)	
ASR	172	196	−24	130	152	−22
OLR	212	221	−9	181	191	−10
Annual						
ALR	73	82	−9	54	65	−11
OLR	189	192	−3	158	160	−2
RDB	−116	−110	−6	−104	−95	−9

of the uncoupled CCM3 simulation of present-day polar climate. It deals with the polar radiation budget simulation. The second paper (Briegleb and Bromwich 1998) deals with the remaining aspects of the polar climate

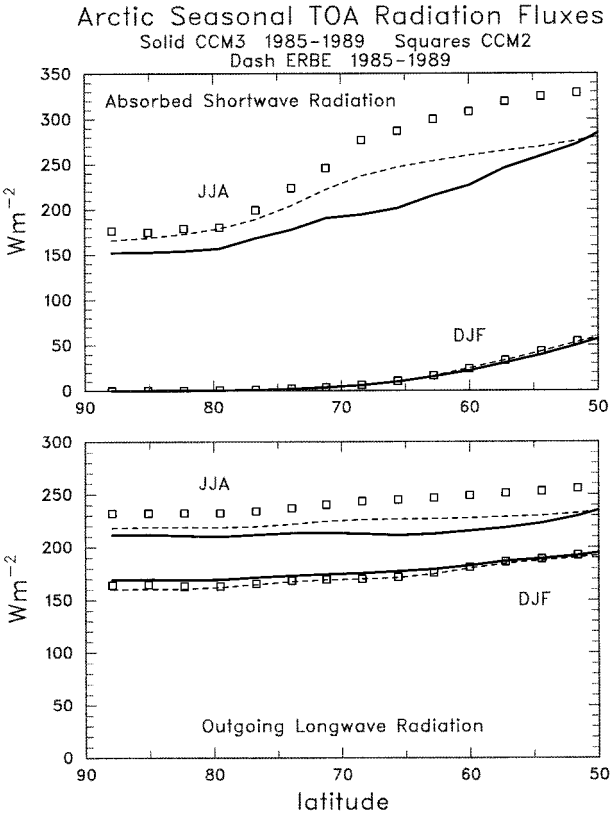

FIG. 2. Ensemble seasonal Arctic TOA radiation fluxes of ASR in the top panel, and OLR in the lower panel. Zonal means are from 50°N to 90°N. The solid line is from the CCM3 AMIP integration over the period 1985–89; the dashed line is the ensemble mean from ERBE data over the same period, and the squares are from CCM2 (case 388, 20-yr ensemble mean).

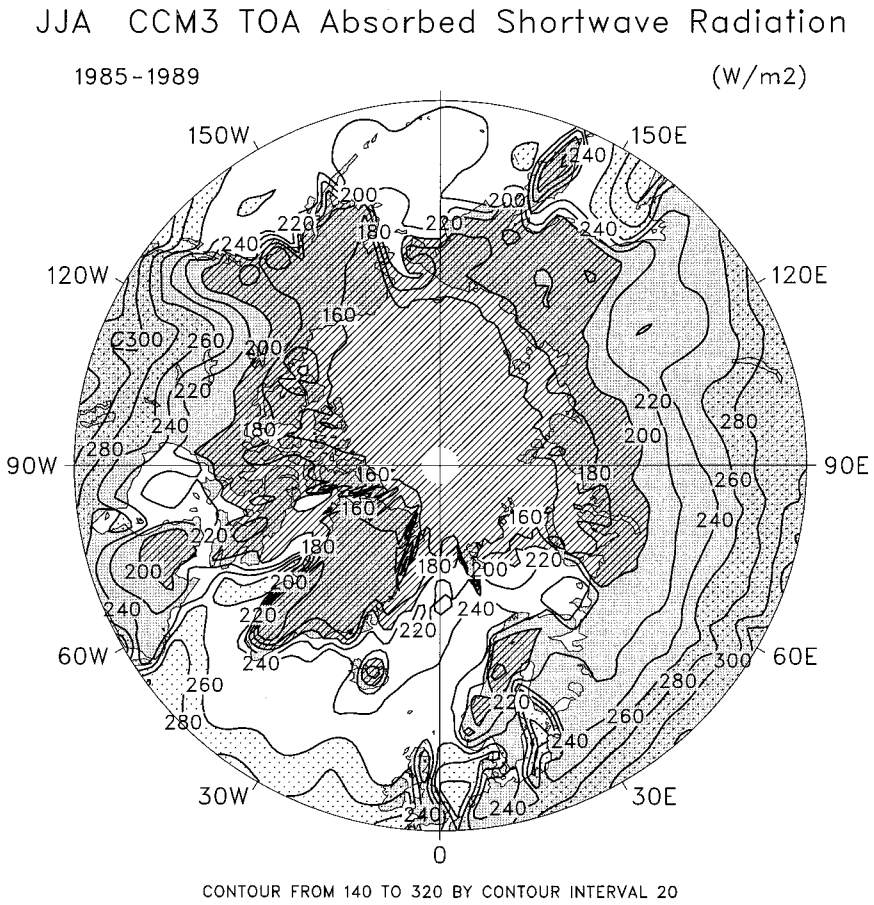

FIG. 3. Summer season (JJA) TOA ASR for the CCM3 AMIP integration over the period 1985–89, W m^{-2} (a), and for the ERBE data for the same period (b). Contour interval is 20 W m^{-2}, with hatching for regions less than 200 W m^{-2} and stippling for regions greater than 260 W m^{-2}.

simulation: the circulation, thermodynamic structure, hydrology, and surface energy budgets.

It is necessary for CCM3 to adequately simulate the climate of the polar regions. Both the Arctic and Antarctic represent large energy sinks important in determining the intensity of the general circulation, and they may be rather sensitive to climate change. Coupling of CCM3 to an ocean/ice model in CSM requires adequate simulations of polar climates, since cold bottom water formation in the polar regions strongly influences the global ocean thermohaline circulation. The radiation budget is a crucial aspect of the polar climate that determines the magnitude of the polar energy sink (Lubin et al. 1998).

Accurately simulating the polar radiation budget is a challenging problem for global climate models. Conditions that are found only in the mid- to upper troposphere in the Tropics and midlatitudes are prevalent throughout the polar troposphere for most of the year. Polar climates are marked by strong seasonal variation in solar insolation, very cold surface temperatures and near-surface inversions, very small water vapor amounts, relatively thin clouds of mixed phase or nearly complete ice, and even a unique phenomenon of clear sky precipitation during winter. High surface albedos and small tropospheric temperature gradients minimize cloud-forcing effects. Curry et al. (1996) present an overview of polar cloud and radiation characteristics.

The polar simulations of previous versions of CCM (CCM1 and CCM2) have been discussed by Battisti et al. (1992), Tzeng et al. (1993), Bromwich et al. (1994), Tzeng and Bromwich (1994), Tzeng et al. (1994), Bromwich et al. (1995), and Williamson et al. (1996). A discussion of the Arctic simulation of CCM2 in particular is found in Bromwich et al. (1994) and in Tzeng and Bromwich (1994), and of the Antarctic simulation in Tzeng et al. (1994). Circulation statistics for CCM2 can be found in Hack et al. (1994), and the simulation of the earth radiation budget in Kiehl et al. (1994). The general conclusion of these papers is that the CCM1 (R15) polar simulations have large biases, particularly in the hydrologic cycle and at low horizontal resolution, whereas the use of semi-Lagrangian water vapor transport and higher horizontal resolution in CCM2 has

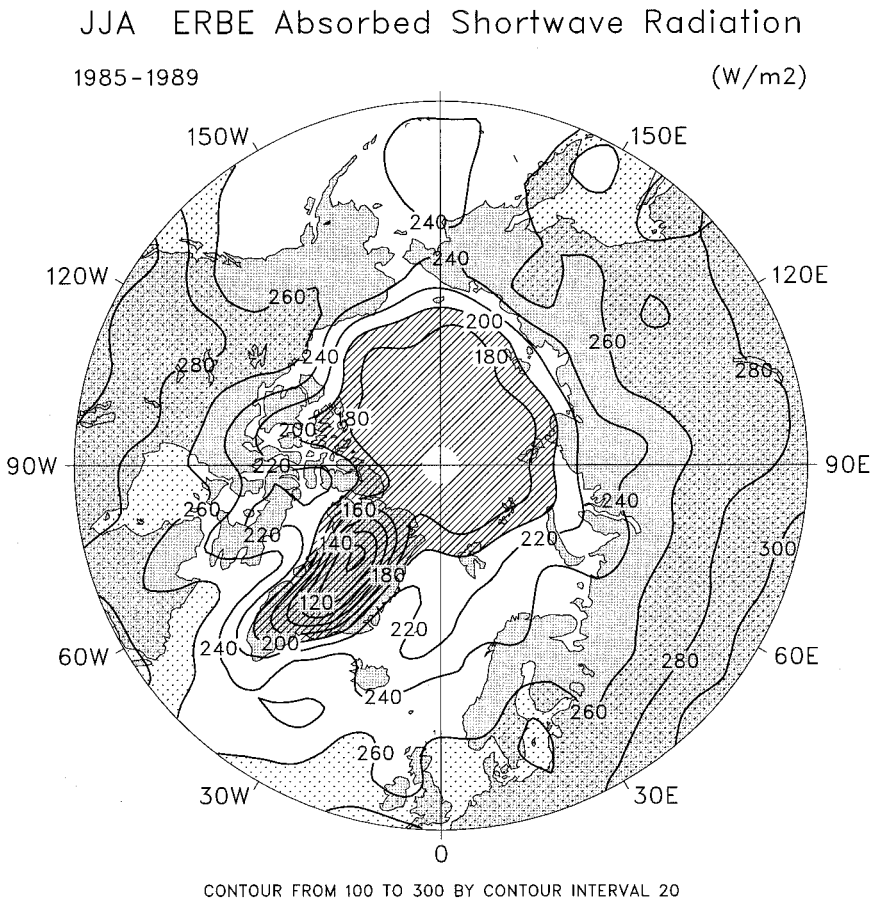

FIG. 3. (*Continued*)

greatly reduced many of these biases. CCM2 simulations have radiation budget biases in mid- and polar latitudes caused by biases in cloud radiative properties.

In this assessment of present-day CCM3 polar radiation budgets, we will make use of the Earth Radiation Budget Experiment (ERBE) data from 1985 to 1989 (Barkstrom and Smith 1986) for the all sky TOA absorbed shortwave radiation (ASR, downward minus upward flux) and the TOA outgoing longwave radiation (OLR). We will also compare the CCM3 TOA polar radiation budget simulation with that of CCM2, the previous version of the CCM. Two other important aspects of the CCM3 radiation budgets considered are the cloud-forcing effects and surface radiation budgets. Validation of these aspects in the polar regions is difficult and bears further discussion.

TOA cloud forcing (CF) is defined as the clear sky flux subtracted from the all sky flux [the sign convention differs between shortwave (SW) and longwave (LW)]. Several studies have shown that polar ERBE CF data for both SW and LW have large uncertainties (Li and Leighton 1991; Nemesure et al. 1994; Yamanouchi and Charlock 1995). This is because the polar snow/ice surface offers little visible, thermal, or microwave contrast with polar clouds, and therefore makes cloud detection difficult. We will use TOA CF results of Curry and Ebert (1992, henceforth CE92) for the Arctic, which used the collocated ERBE and National Oceanic and Atmospheric Administration (NOAA) satellite measurements of Li and Leighton (1991) to check their model calculations, and those of Yamanouchi and Charlock (1995) for the South Pole, which used collocated ground observations to interpret the TOA fluxes accurately.

There are at least three approaches to validating CCM3 surface radiation fluxes: 1) use surface observations at selected stations (such as Wild et al. 1995; Dutton et al. 1989, henceforth D89); 2) use results from sophisticated one-dimensional model calculations, which employ realistic values of input data (CE92); and 3) use estimates of surface radiation fluxes based on satellite or other (i.e., analyzed) data (such as Li and Leighton 1993, henceforth LL93; Schweiger and Key 1994). Concerning the third approach, LL93 estimated global SW surface absorption based on a theoretical algorithm relating surface absorption to TOA reflection, depending only on solar zenith angle μ and precipitable water (PW) (Li et al. 1993a; Li et al. 1993b). The algorithm was used to estimate surface and atmospheric

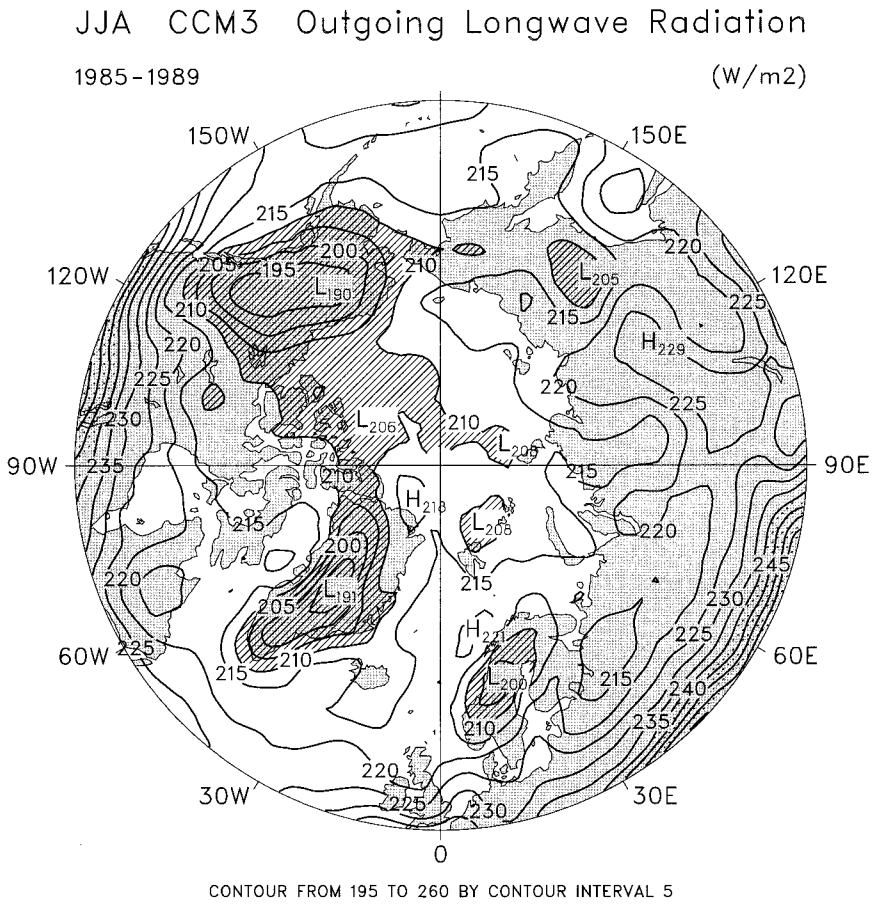

FIG. 4. Summer season (JJA) OLR for the CCM3 AMIP integration over the period 1985–89, W m^{-2} (a), and for the ERBE data for the same period (b). Contour interval is 5 W m^{-2}, with hatching for regions less than 210 W m^{-2} and stippling for regions greater than 240 W m^{-2}.

SW absorption from 5 yr of ERBE data (LL93). The basic assumption in this approach is that the fraction of TOA solar irradiance absorbed in the atmosphere (for given μ and PW) is independent of cloud conditions. Given the recent concern over enhanced shortwave cloud absorption (Kiehl et al. 1995), which would invalidate the basic assumptions of LL93, this dataset is not used for comparison with CCM3. Schweiger and Key (1994) estimate TOA and surface flux–cloud forcings using International Satellite Cloud Climatology Project cloud data, along with a radiative transfer model. Their results were similar to those of CE92. The Global Energy Budget Archive (GEBA) dataset used by Wild et al. (1995) is not generally available. Therefore, for the South Pole the surface measurements of D89 are employed. For the Arctic, the modeling results of CE92 are employed. Despite the model assumptions in the CE92 study, much observational data concerning clouds and their optical properties were used. Thus, we consider this to be a reasonable validation dataset.

In section 2, the relevant CCM3 physics and the observations for model assessment are discussed. In section 3, the assessment of the polar radiation budget simulation of CCM3 is presented. Section 4 concludes with a summary of the suggested improvements.

2. Model and observations

a. Model

The most recent version of the NCAR CCM is version three: CCM3. A general description of CCM3 can be found in Kiehl et al. (1998a), and a complete description of the physics of CCM3, along with numerical approximations, can be found in Kiehl et al. (1996). CCM3 includes several improvements over the previous version (CCM2), although many aspects of the model formulation and implementation are identical to those of CCM2. The standard version of CCM3 continues to be T42 (triangular truncation at wavenumber 42) horizontal resolution (about 2.8° lat × 2.8° long) with the same 18 vertical hybrid coordinate levels as in CCM2. CCM3 continues to employ the semi-implicit–leapfrog time integration scheme, spectral transform method for treating the dry dynamics, a biharmonic horizontal diffusion operator, and a semi-Lagrangian scheme for transporting

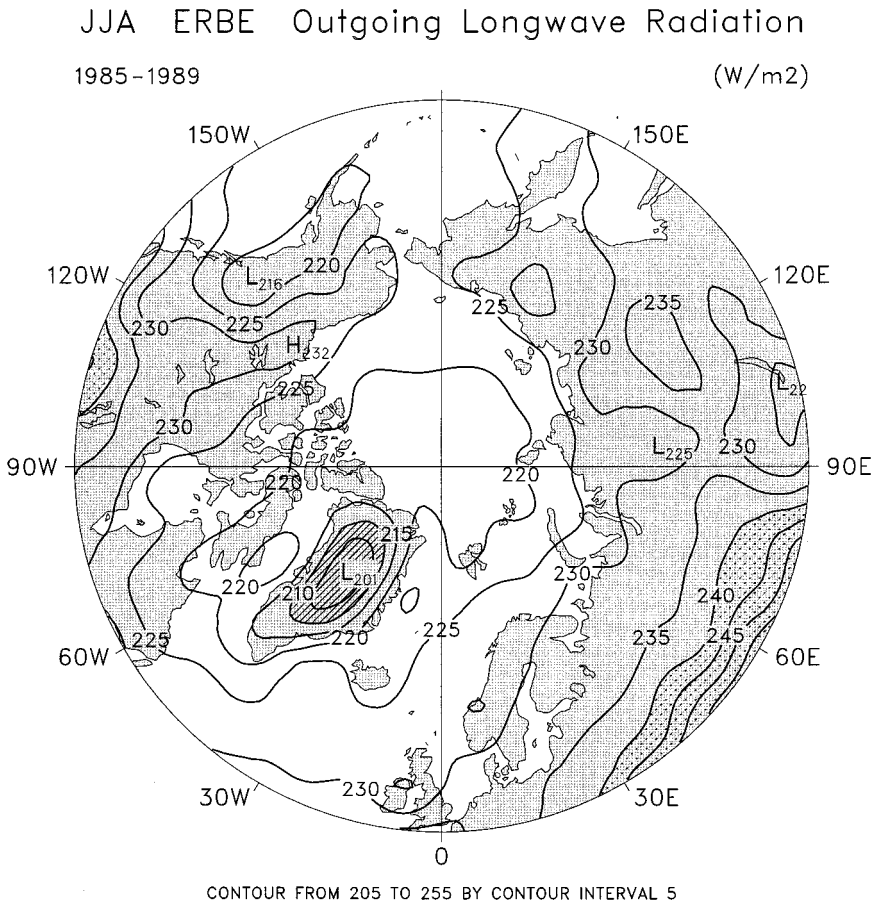

FIG. 4. (*Continued*)

water vapor. Modifications to the physical parameterizations of CCM2 were motivated both by the desire to reduce systematic simulation errors in CCM2, particularly in top-of-atmosphere and surface energy budgets, as well as to make the model more suitable for coupling to alternative surface (land, ocean, ice) component models. We briefly summarize CCM3 cloud, radiation, and surface physics important for polar processses.

Cloud fraction A_c is computed diagnostically depending on relative humidity, vertical motion, and boundary layer stability. In-cloud water path (CWP, g m^{-2}) is determined diagnostically based on the total column precipitable water vapor (PW, kg m^{-2}) as CWP $= \int \rho_l \, dz$, where z is height and ρ_l is the in-cloud water concentration, $\rho_l = \rho_l^0 e^{-z/h_l}$, $\rho_l^0 = 0.21$ g m^{-3}, and the cloud water scale height (m) is $h_l = 700 \ln(1 + \text{PW})$. Cloud particle ice fraction (f_{ice}) is temperature dependent, with value 0 for air temperature greater than -10°C, linearly increasing to a value of 1 for air temperatures below -30°C. Cloud particle size (r_e, effective radius) is dependent on surface type and phase. For liquid water clouds, the effective radius r_{el} is 10 μm over ocean, and $r_{el} = 5(1 + f_{ice})$ μm over land. For ice clouds, r_{ei} is 10 μm for atmospheric pressure greater than 0.8 of surface pressure, increasing linearly with decreasing pressure to 30 μm for pressures less than 0.4 of surface pressure. Both shortwave and longwave cloud particle optical properties depend on phase. Optical properties are specified separately for liquid and ice, and weighted by the ice fraction (f_{ice}). In the shortwave, the in-cloud extinction optical depth τ is distinguished between liquid phase τ_l and ice phase τ_i: $\tau_l = \text{CWP}(a_l + b_l/r_{el})(1 - f_{ice})$ and $\tau_i = \text{CWP}(a_i + b_i/r_{ei}) f_{ice}$, where the a, b coefficients depend on phase and spectral interval. In the longwave, the cloud emissivity is $\epsilon_{cld} = 1 - e^{-1.66\kappa_{abs}\text{CWP}}$, where the longwave absorption coefficient (m^2 g^{-1}) is $\kappa_{abs} = \kappa_l(1 - f_{ice}) + \kappa_i f_{ice}$ and κ_l is a constant liquid coefficient, while the ice coefficient κ_i varies inversely as the ice effective radius r_{ei}.

CCM3 SW radiative transfer model is based on the δ-Eddington approximation for multiple scattering in a plane-parallel atmosphere. Eighteen spectral intervals were employed to account for O_3, H_2O, O_2, CO_2, cloud particle absorption, and molecular/aerosol/cloud particle/surface scattering. Spectral optical properties for each of the 18 vertical atmospheric layers are evaluated assuming homogeneous mixing. Layer fractional cloud cover is included by weighting cloud optical depths (in

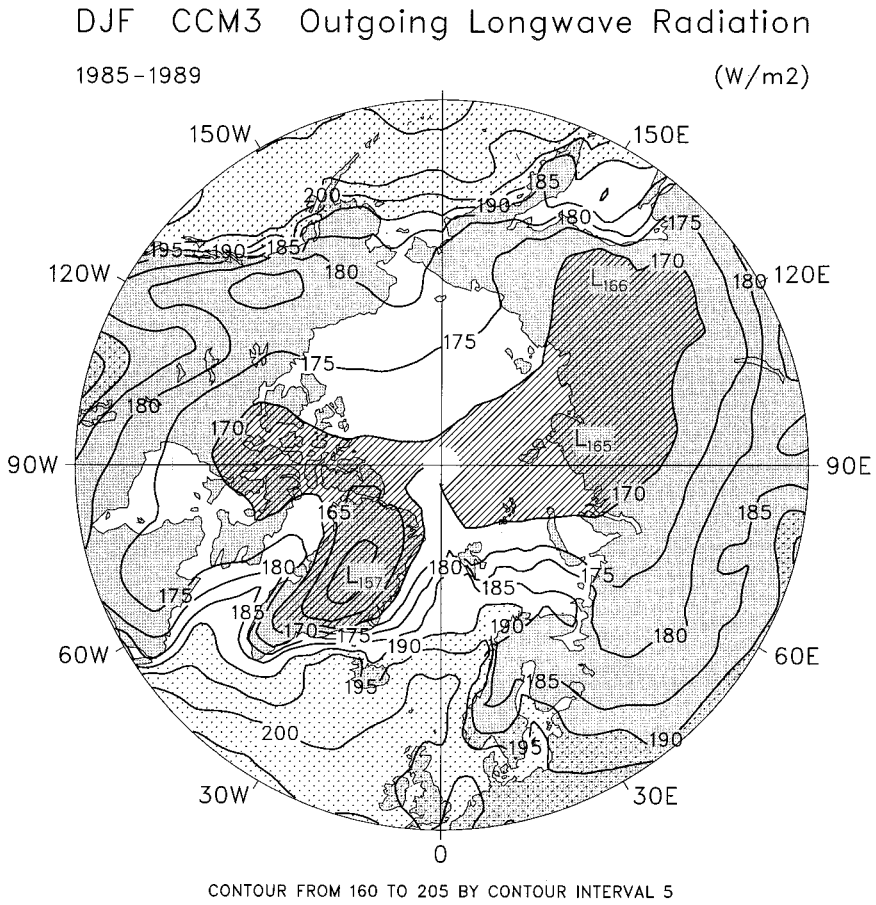

FIG. 5. Winter season (DJF) OLR for the CCM3 AMIP integration over the period 1985–89, W m^{-2} (a), and for the ERBE data for the same period (b). Contour interval is 5 W m^{-2}, with hatching for regions less than 170 W m^{-2} and stippling for regions greater than 190 W m^{-2}.

turn dependent on cloud water/ice paths) by cloud fraction[2/3], an empirical approximation roughly comparable to a random overlap assumption. Cloud particle properties depend on cloud particle size and on phase. A background globally uniform aerosol is assumed in the boundary layer. Surface albedos depend on spectral interval and on whether direct or diffuse radiation is incident. The δ-Eddington reflectivities/transmissivities for each layer are vertically added (including the surface) to account for interlayer multiple scattering, distinguishing direct and diffuse radiation. Broadband SW fluxes are sums of spectral fluxes.

CCM3 LW radiative transfer model is based on an emissivity formulation for the rotation and 6.3-μm vibration bands of H_2O, and a band absorptance formulation for the 15-, 10.4-, and 9.4-μm bands of CO_2; the 9.6-μm band of O_3; and the major bands of CH_4, N_2O, CFC11, and CFC12. Band overlap is accounted for. The atmosphere is assumed to be plane-parallel, and atmospheric scattering is ignored. Fractional cloud cover is included for each vertical layer assuming random cloud overlap. Cloud emissivity effects are included by reducing layer cloud fractions to the equivalent black cloud fraction (i.e., $A_c' = \epsilon_{cld} A_c$).

CCM3 SW and LW radiation are computed every model hour and held fixed in between. In the LW, the time-consuming gaseous transmissions are computed only once every 12 model hours, however. Thus, the effects of rapidly varying clouds are included for both SW and LW radiation, and the diurnal cycle of solar radiation is well resolved.

The surface polar physics of CCM3 is summarized as follows. Over land, the surface conditions are represented by the Land Surface Model (LSM) of Bonan (1996). Snow is determined by a simple mass balance between gains from snowfall and surface deposition of vapor to liquid and to solid, and losses from snowmelt and sublimation. The horizontal fraction of ground covered with snow is proportional to the snow mass for snow depths below 5 cm, above which the fraction is one. Snow masking of vegetation depends on the leaf area index. Glacier albedos are distinguished from frozen lake and wetland albedos. Soil albedos depend on the volumetric water content of the first soil layer. Long-

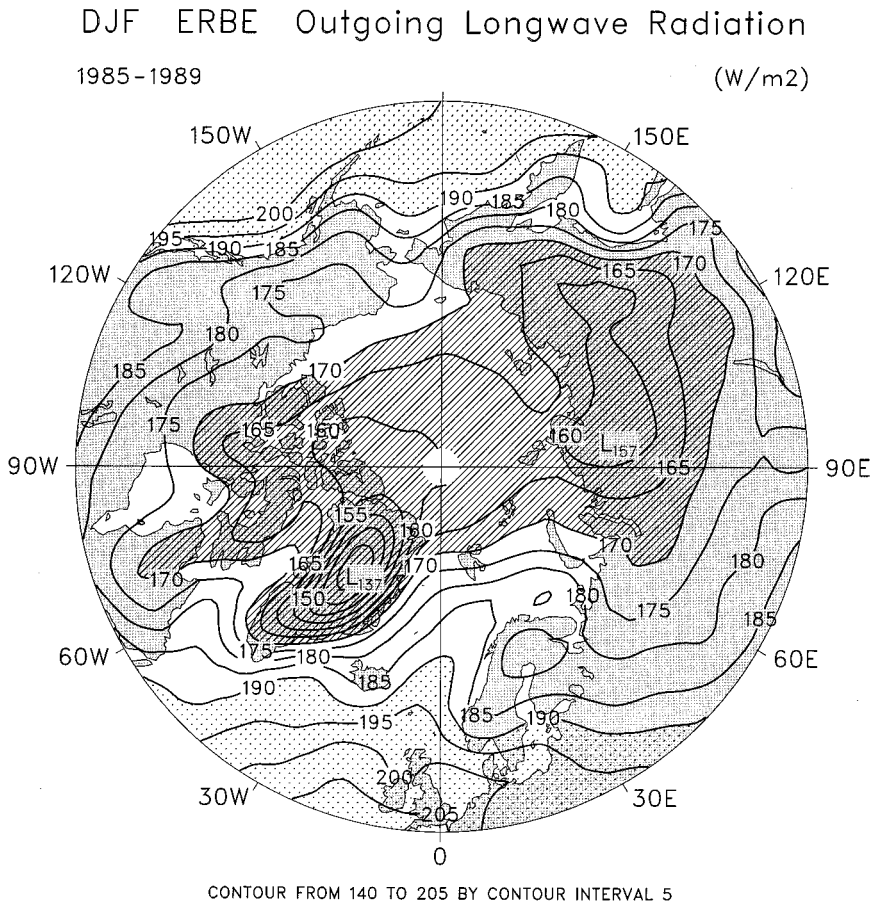

FIG. 5. (*Continued*)

wave emissivity over soil and wetland surfaces is 0.96, while it is 0.97 over snow, glacial ice, and lakes.

Over ocean the prescribed ocean temperatures are linearly interpolated between monthly mean values. Whenever the SST is less than the minimum −1.8°C, sea ice conditions are assumed. Sea ice is represented by a constant thickness slab of 2-m water ice, which completely covers the ocean grid box, overlain with a constant uniform layer of 0.005-m (liquid water equivalent) snow, with initial ice temperatures at freezing. The ice temperatures are then computed using a four-layer diffusion model with constant layer thicknesses of 50 cm and a constant ocean lower boundary freezing temperature, thus allowing for heat exchange with the underlying ocean. The top snow/ice-layer mixture assumes snow overlying ice and distinguishes the thermal conductivities of snow and ice. The top layer ice temperature is used to compute surface flux exchange with the atmosphere. Surface aerodynamic roughness of ice is constant. Sea-ice/snow composite albedos allow for partial coverage of the ice by overlying snow, but are constant in time. In particular, they are independent of temperature (i.e., no summer melt ponds). The constant broadband snow albedo is 0.83, that of bare sea ice 0.59, and the composite 0.66. Both ocean and sea ice have longwave emissivities of 1.

The CCM3 polar climates discussed in this paper are those simulated by an integration from January 1979 through August 1993, known as the AMIP integration (Atmospheric Model Intercomparison Project; Gates 1992). This AMIP integration prescribes monthly mean SSTs and implied sea-ice distribution as ocean boundary conditions for CCM3. As noted above, the sea-ice distribution is implied by the lowest SSTs in this dataset. It is pertinent to discuss the seasonal and interannual representation of sea-ice extent in this AMIP SST dataset.

The inferred sea-ice extent for each month over the entire period (1979–93) is shown in Fig. 1 for both the Arctic and the Antarctic. Also shown are the ice extents inferred from the monthly blended SST data of Reynolds and Marsico (1993), as well as those inferred from satellite passive microwave data by Gloersen et al. (1992). (Note that Fig. 1 shows ice extents, *not* areas, and therefore assumes complete horizontal coverage throughout the interior of the ice pack.) It is not known if the AMIP data made use of some of the same SST data that Reynolds and Marsico (1993) did, but there

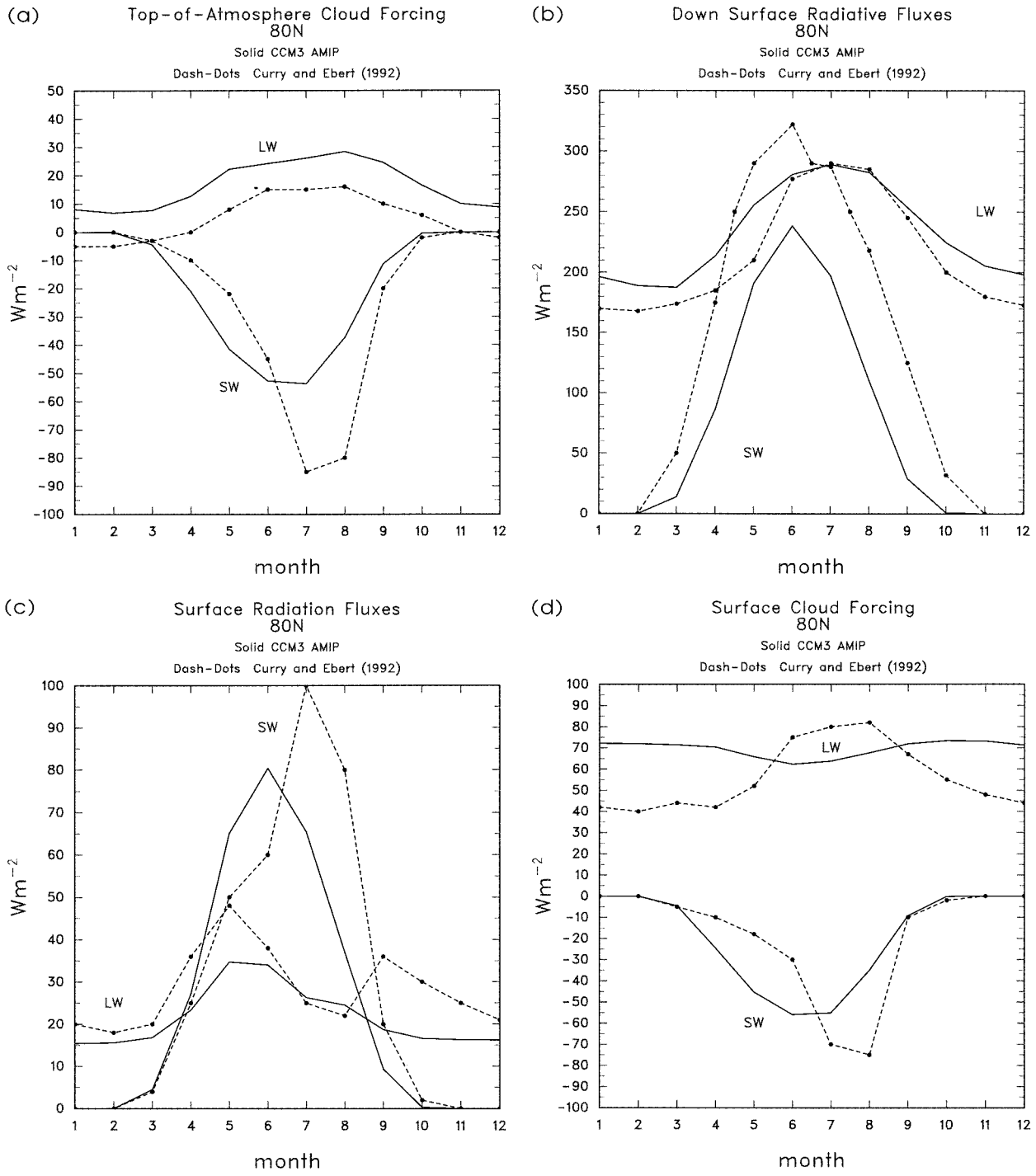

FIG. 6. Annual cycle of 80°N (a) TOA cloud forcing, (b) surface downward SW and LW fluxes, (c) net surface SW and LW radiation fluxes, and (d) surface cloud forcing. Solid, CCM3 AMIP (1979–93). The dash–dotted line represents data from Curry and Ebert (1992).

should be some consistency between the datasets, and there is. The realistic seasonal cycle of ice extent in each hemisphere is obvious, as is the nonphysical jumps in the ice extent, particularly after January 1982 in both hemispheres and after 1988 in the Southern Hemisphere. These jumps suggest changes in sources and/or analysis procedures in the original data used for the AMIP composite. In the case of the blended Reynolds and Marsico (1993) analysis, prior to January 1982 only in situ ice data were used, from January 1982 to December 1987 data from the University of Maryland, and after January 1988 data from the U.S. Navy–NOAA joint ice center.

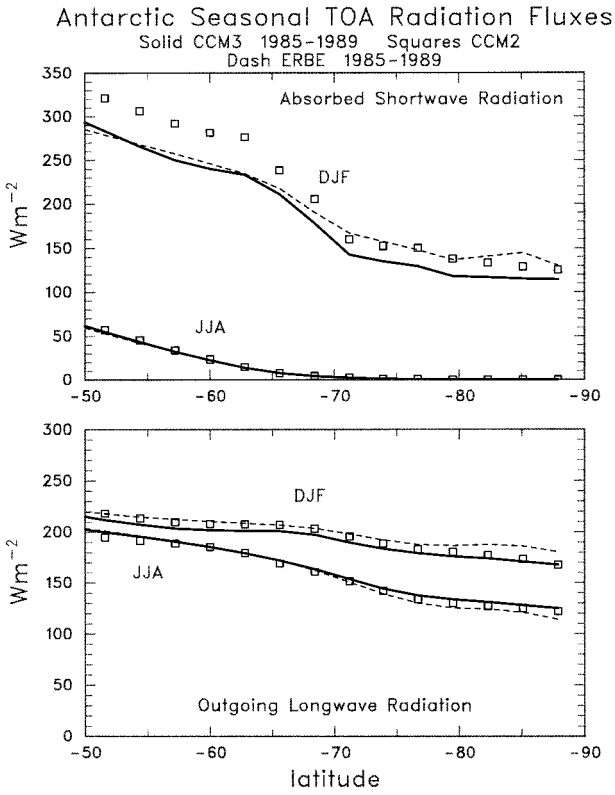

FIG. 7. Same as Fig. 2 except for the Antarctic.

Note that the Gloersen et al. (1992) data have no discernable trends. Despite these jumps in ice extent, the AMIP integrations still represent a first attempt at including the effects of seasonal and interannual variations in ice extent on the atmospheric simulation. Maps of monthly ice extent (not shown) disclose realistic geographic distribution of ice over time. Year-to-year variations in ice are thus confined to ice extent (and not of course, ice concentration, thickness, type, or surface albedo).

b. Observations

The observations used for assessing the CCM3 polar TOA radiation budget simulations were taken from the ERBE data over 1985–89 (Barkstrom and Smith 1986). We considered annual and winter/summer season radiation budgets. The winter season (DJF = December–February) ensemble consisted of the four (northern) winters from 1985 through February 1989; the summer season (JJA = June–August) ensemble included the five (northern) summers from 1985 through 1989. Annual ensemble means were constructed from all available monthly means during the calendar years of 1985 through 1989. We note that the ensemble, annual, and global mean radiation balance of the ERBE data over this period is $+4.7$ W m^{-2}. [Note that this differs from the $+3.3$ W m^{-2} in Kiehl et al. (1998b) because of differences in the procedure used to fill in missing data and in defining ensemble monthly and annual means.] It is not known whether this large imbalance is realistic, or whether either or both the ERBE SW or LW radiation budgets have systematic biases. The regional accuracy of the ERBE data is estimated to be ± 7 W m^{-2} (Harrison et al. 1990). Thus, we consider large-scale systematic differences larger than 5–7 W m^{-2} to be significant.

For comparison with CCM3 simulated clouds, we used the data of Hahn et al. (1987), consisting of surface cloud observations from the periods 1971–81 over land and 1952–81 over ocean, on a 5° lat $\times$ 5° long grid. All available years were averaged into mean total and low cloud covers. The low category combined all stratus, cumulus, and cumulonimbus observations; the total included all cloud types. A conservative estimate of the random uncertainties in these observed fractional cloud covers would be ± 0.05. Recently it has been shown that cloud covers based on surface observations are *under reported* at night due to poor illumination (Hahn et al. 1995). Segregation of cloud observations between illuminance by moonlight and darker conditions reveals a global bias of -0.02. Larger biases during polar night are in the range of -0.05 to -0.10.

For the surface radiation budgets in the Arctic Ocean, the results of modeling experiments from CE92 were used. In that study, the annual cycle of cloud optical properties (partially based on available measurements) were determined so that the computed TOA and surface radiation fluxes compared favorably with available data. The computed annual cycles of surface temperature and surface albedo were quite realistic. A latitude of 80°N was used for computing the annual cycle of solar insolation. Despite the modeling nature of these data, they represent a self-consistent set of data useful for validation.

For the surface radiation budgets in the Antarctic, we used the measurements made at the U.S. Amundsen Scott South Pole Station (90°00′S, 2835 m above mean sea level) by the NOAA Geophysical Monitoring for Climatic Change (D89). The direct, global (all sky), and reflected SW, and the downward and upward LW fluxes were measured. The instruments were well maintained and frequently calibrated. The downward fluxes were measured at 10-m height at a distance sufficiently removed from other structures to allow a nearly unobstructed 2π steradian view of the horizon. The upward fluxes were measured 1–2 m above a clean snow surface. Monthly flux and daily summaries were used. Because Amundsen Scott Station is surrounded by an almost featureless snow–ice plane for nearly 300 km in all directions, the data are considered representative of the continental interior plateau.

3. Assessment of CCM3 polar radiation budget simulation

a. Arctic radiation budget

Table 1 shows comparisons of the ensemble (1985–89) area-averaged polar cap (70°–90° N) TOA ASR and

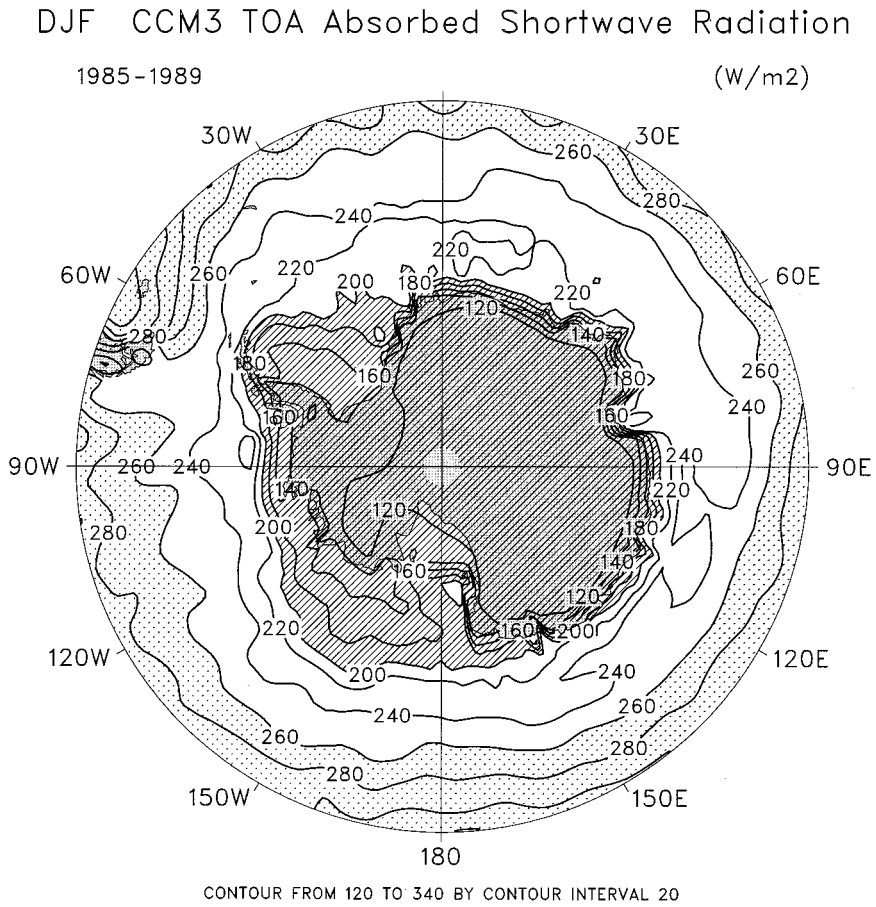

FIG. 8. Same as Fig. 3 except for the Antarctic summer (DJF) season.

OLR for both CCM3 and ERBE data. Annual means and seasonal (DJF, JJA) values are tabulated. During winter (DJF), CCM3 OLR exceeds the data by 7 W m^{-2}, whereas during summer (JJA) it is less than the data by 9 W m^{-2}. During summer (JJA), CCM3 has a lower ASR by 24 W m^{-2} (note that, as mentioned previously, to achieve an annual global radiation balance in the ERBE data, either one or both of the ASR and OLR would need to be reduced by a total of 4.7 W m^{-2}). On an annual basis, CCM3 OLR is slightly less than the ERBE data by 3 W m^{-2}, whereas the ASR is less than ERBE by 9 W m^{-2}, yielding a lower net radiation balance in CCM3 of 6 W m^{-2}.

Figure 2 compares the zonal and seasonal mean ASR and OLR for CCM3 and ERBE data. Also shown are CCM2 fluxes. The differences between CCM3 and ERBE data noted above are mostly prevalent throughout the Arctic during the respective seasons. Note though that the difference in ASR for JJA is largest between 60°N and 70°N but diminishes to zero at 50°N. This negative ASR bias is also seen in Kiehl et al. (1998b), in terms of the TOA albedo differences of order -0.02 to -0.09. CCM3 OLR has a reduced annual cycle compared to the ERBE data.

Figures 3a,b compare the regional ASR for JJA between CCM3 and ERBE data. (Regional random uncertainties in the ERBE ASR are less than ± 7 W m^{-2}.) Noteworthy is the extension of the region of low ASR from the Arctic Ocean into the surrounding polar land regions. Note the strong regional gradients in CCM3 ASR that follow polar coastlines, especially along eastern Siberia and the southern Alaska–Pacific coast of Canada, and also as far south as Norway and Newfoundland. Not until the outer edge of the plots (50°N) is reached do the CCM3 and ERBE ASR become comparable, with the exception of a few ice-free ocean regions in the North Atlantic.

Figures 4a,b compare the regional OLR for JJA between CCM3 and ERBE data. As noted in Table 1 and Fig. 2, CCM3 OLR is generally less than the ERBE OLR by 10 W m^{-2} in the central Arctic. The regional patterns of ERBE OLR are only roughly simulated by CCM3. In particular, the region of Alaska and northwest Canada, extending across the Canadian Archipelago to Greenland, and including Scandinavia, has CCM3 OLR at least 15 W m^{-2} less than the ERBE data. Figures 5a,b show the comparison of OLR for DJF. The low OLR region following the polar vortex (see Briegleb and

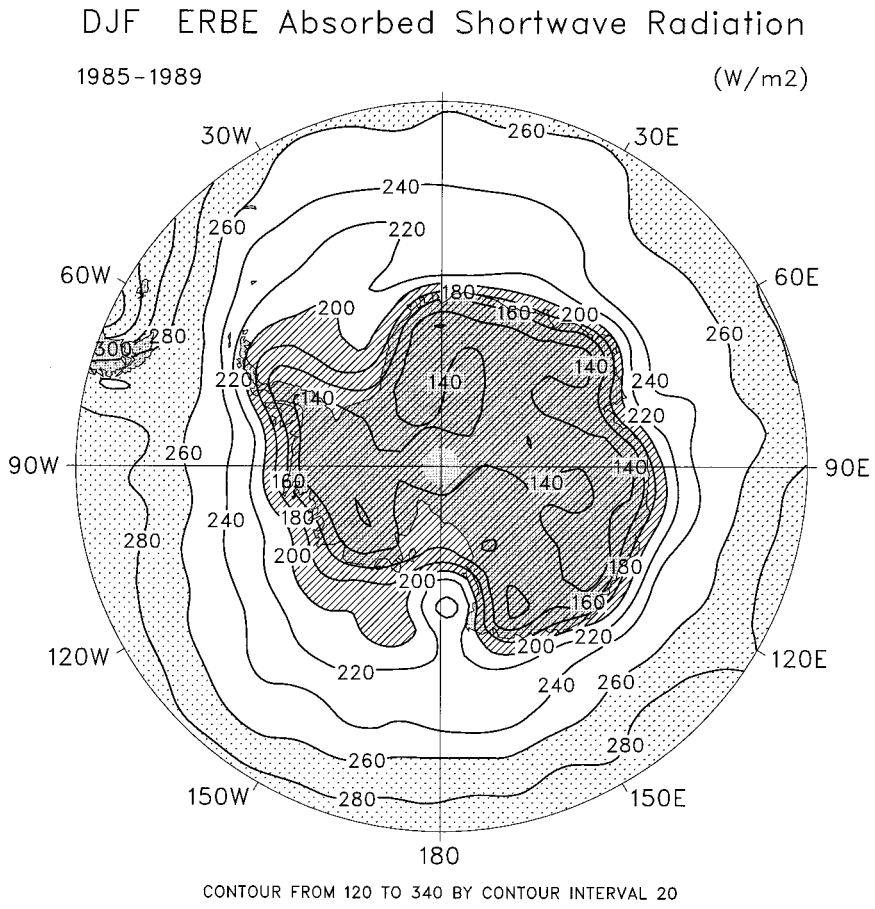

FIG. 8. (*Continued*)

Bromwich 1998) is well simulated by CCM3, although the OLR is systematically high by 5–10 W m^{-2} over the entire Arctic Basin.

We note that these results are in contrast with those of CCM2, as presented in Kiehl et al. (1994). In CCM2, excess ASR occurs over all land regions surrounding the Arctic Ocean (see Fig. 2) due to biases in cloud properties (cloud fraction, particle size, and water path). Likewise, excess OLR in CCM2 occurred, due both to the biases in cloud properties as well as to a summer warm bias in atmospheric and surface temperatures in response to the excessive ASR. That CCM3 has perhaps overcorrected for the excessive ASR (and to a lesser extent the OLR) will be discussed at the end of this section. Figure 2 shows that CCM2 summer ASR and winter OLR from 70°N to the North Pole are in closer agreement with the ERBE data than are those of CCM3.

Figure 6a shows CCM3 80°N mean annual cycle of TOA cloud radiative forcings, along with those estimated by CE92. The CFs are defined so that negative values imply clouds cool the system, while positive values imply that they heat [thus, shortwave cloud forcing (SWCF) = ASR (all) − ASR (clear); longwave cloud forcing (LWCF) = OLR (clear) − OLR (all)]. The CCM3 TOA SWCF is less than CE92 in spring and greater in late summer and early fall, consistent with seasonally invariant sea ice albedo. The CCM3 TOA LWCF is systematically larger than CE92 by 10–15 W m^{-2}, with positive values at all times of the year. Figure 6b shows the CCM3 mean annual cycle of surface downward fluxes, compared to those of CE92. CCM3 has considerably less downward SW flux, as much as 50–70 W m^{-2}, whereas its LW downward exceeds the CE92 values by 15–25 W m^{-2} except for the summer season. Figure 6c shows the net surface radiation fluxes. CCM3 SW absorption is generally less than CE92 by 20–50 W m^{-2} (except for spring) again consistent with seasonally invariant sea ice albedos. The broadband surface albedo of CCM3 is 0.66, which is less than the CE92 spring value of 0.80, and larger than the late summer values of 0.50. The LW net surface flux (upward minus downward) of CCM3 is less than CE92 by 5–10 W m^{-2}, except for July and August. Figure 6d shows the surface CFs, which are defined in the same manner as those for the TOA [thus, SWCF = Net SW (all) − Net SW (clear); LWCF = Net LW (clear) − Net LW (all); net fluxes are downward minus upward for SW and upward minus downward for LW]. CCM3 SWCF

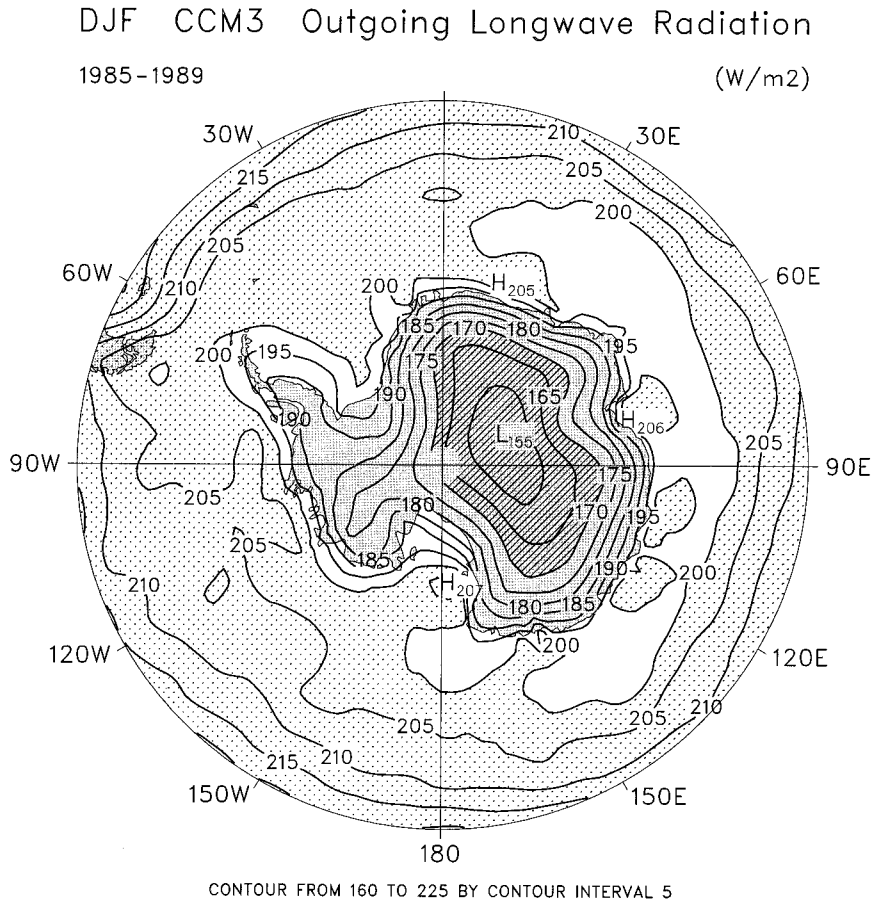

FIG. 9. Same as Fig. 4 except for the Antarctic summer (DJF) season. Hatching for regions less than 170 W m^{-2} and stippling for regions greater than 200 W m^{-2}.

shows the same seasonal asymmetric bias already noticed in the TOA and SW surface absorption. The CCM3 LWCF is larger than CE92 during winter and less during summer, consistent with the minimal seasonal amplitude of TOA OLR already noted.

b. Antarctic radiation budget

Table 1 also shows comparisons of the ensemble (1985–89) area-averaged polar cap (70°–90°S) TOA ASR and OLR for both CCM3 and ERBE annual and seasonal data. Interestingly, the biases in CCM3 ASR and OLR compared to ERBE data are of similar sign and mostly similar magnitude as for the Arctic. During winter (JJA), CCM3 OLR exceeds the data by 6 W m^{-2}, whereas during summer (DJF) it is less than the data by 10 W m^{-2}. During summer (DJF), CCM3 has lower ASR by 22 W m^{-2}. On an annual basis, CCM3 OLR is slightly less than the ERBE data by 2 W m^{-2}, whereas the ASR is less than ERBE by 11 W m^{-2}, yielding a lower net radiation balance in CCM3 of 9 W m^{-2}. So, with slight differences (order 2–3 W m^{-2}), the comparison for the Antarctic is the same as for the Arctic.

Figure 7 compares the zonal seasonal TOA radiation budgets for the Antarctic. As for the Arctic, the zonal and seasonal mean differences in ASR and in OLR are prevalent over much of the Antarctic, although the differences in ASR in DJF and in OLR for JJA are mostly gone north of 60°S lat (i.e., once away from the Antarctic continent). The difference in OLR during DJF is prevalent out to latitude 50°S. Note that CCM2 summer ASR over the Antarctic continent, and CCM2 OLR over the entire region, are closer to the ERBE data than are those of CCM3. Examination of Figs. 8a,b comparing the regional ASR for summer (DJF) discloses the low ASR over both the continent and the adjacent ocean regions that are mostly ice free. This negative ASR bias is also seen in Kiehl et al. (1998b), in terms of the TOA albedo differences of order +0.05.

Figures 9a,b compare the regional OLR for DJF between CCM3 and ERBE data. As noted in Table 1 and Fig. 7, CCM3 OLR is generally less than the ERBE OLR by 10 W m^{-2}. The regional patterns of ERBE OLR are reasonably simulated by CCM3. In particular, the ERBE OLR patterns following the topography of the

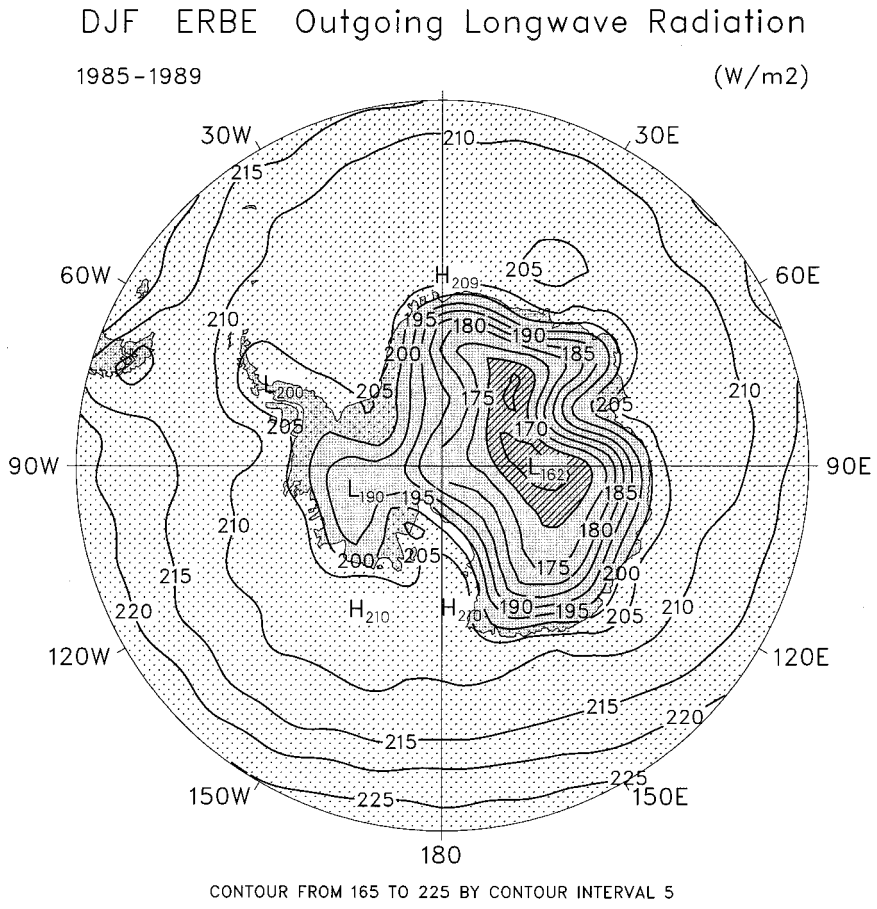

FIG. 9. (*Continued*)

Antarctic continent are captured quite well by CCM3, especially in east Antarctica.

Figures 10a,b show the comparison of OLR for JJA. The CCM3 OLR and the ERBE data agree mostly to within 6 W m^{-2}, as is the case for the Arctic. In particular, the low OLR region following the polar vortex (see Briegleb and Bromwich 1998) over east Antarctic topography is well simulated by CCM3, although the OLR is high by 10–15 W m^{-2}. In general the winter season latitudinal gradient in OLR from 50°S to the South Pole is not as great in CCM3 as in the ERBE data.

As mentioned for the Arctic, these CCM3 ASR and OLR results are in contrast to those of CCM2 (see Fig. 7). In CCM2, excess ASR occurs over all ocean regions surrounding the Antarctic continent, due to biases in cloud optical properties (particle size and liquid water path), as for the Arctic. For the OLR, however, CCM3 and CCM2 have approximately the same biases compared to the ERBE data—namely, too much winter (JJA) emission and too little summer (DJF) emission—except that CCM2's biases are smaller.

Figure 11a shows the CCM3 South Pole mean annual cycle of TOA cloud radiative forcings (the equivalent data are not available). The TOA SWCF is negative for all months of solar illumination, indicating that addition of clouds increases TOA albedo, in accordance with the studies of Nemesure et al. (1994) and Yamanouchi and Charlock (1995), and contrary to initial ERBE data. These studies carefully collocated ERBE SW pixel measurements with near-surface SW measurements to demonstrate this. The TOA LWCF is small and positive during southern summer, but becomes small and negative during southern winter. This unique negative TOA LWCF was noted by Yamanouchi and Charlock (1995) (although a similar signature is evident in the modeling studies of CE92 shown in Fig. 6a).

Figure 11b shows the CCM3 South Pole mean annual cycle of surface downward shortwave and longwave fluxes, compared to those of D89, based on limited surface radiation measurements during April 1986 through January 1988. Note that the months are numbered starting with July as 1. The absolute largest estimated uncertainty in the measured SW flux is 9 W m^{-2}, and in the measured LW flux 7.5 W m^{-2}. CCM3 SW downward flux is systematically smaller than the surface measurements, around 50 W m^{-2} during peak illumination in December. The CCM3 LW downward flux is about 10–

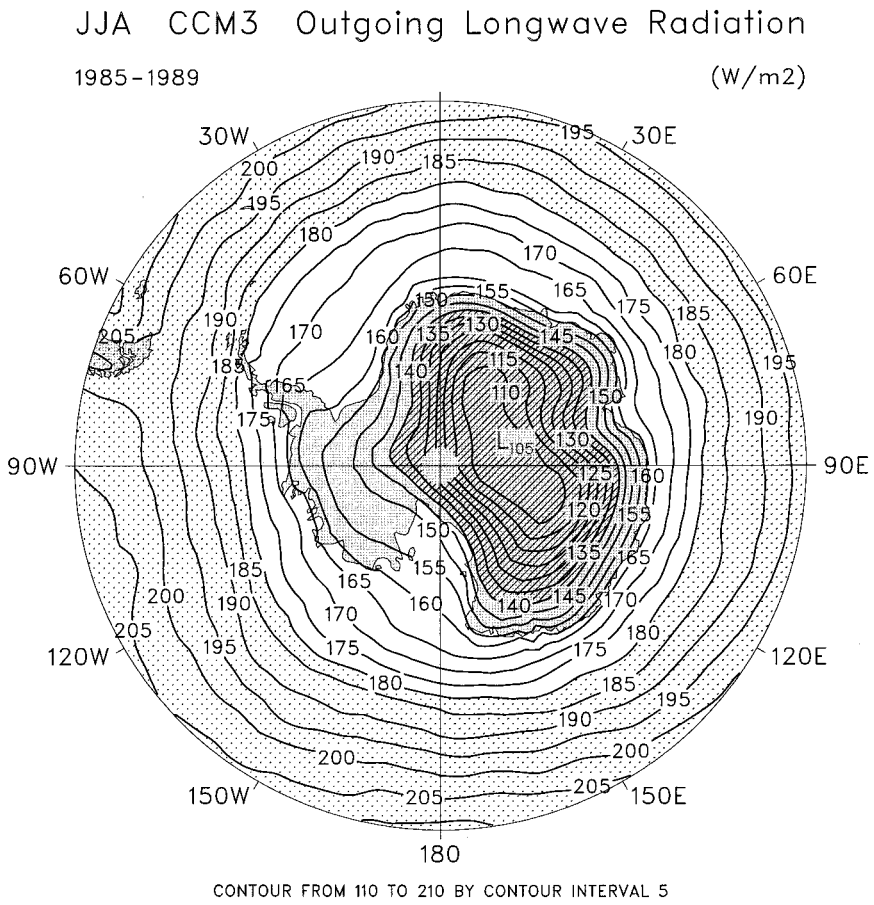

FIG. 10. Same as Fig. 5 except for the Antarctic winter (JJA) season. Hatching for regions less than 140 W m^{-2} and stippling for regions greater than 180 W m^{-2}.

20 W m^{-2} larger than the surface observations for all months except December and January.

Figure 11c shows the CCM3 South Pole mean surface radiation budgets. The CCM3 SW absorption is systematically smaller than the surface observations by 10–15 W m^{-2}. In contrast to the Arctic, the SW absorption remains less than the observations for all months. CCM3 broadband surface albedo is an invariant 0.84, while those inferred from the D89 data were mostly between 0.79 and 0.82. Thus about half of the surface negative bias in SW absorption is due to too high a surface albedo. The LW surface cooling is larger than the surface observations during winter by 5 W m^{-2}, smaller during early summer by 5 W m^{-2}, and agrees during January and February.

Figure 11d shows the South Pole surface CFs for CCM3 and the observations. The CFs from the observations were estimated for each month by using the maximum ASR and minimum OLR (upward minus downward) for clear sky. CCM3 SWCF at the surface is somewhat larger than that of the observations, while the LWCF is significantly larger by about 40 W m^{-2} compared to the observations.

c. *Cloud fraction*

Biases in cloud cover could produce the ASR and OLR biases. Figures 12a,b, and 13a,b compare zonal-mean January and July cloud fractions, for both total and low (1000–700 hPa in CCM3) cloud covers for the Arctic and Antarctic, respectively. Over the Antarctic plateau, surface pressures are around 700 hPa, so the zonal means of Figs. 13a,b are for those longitudes where surface pressures are greater than 700 hPa. The cloud observations are from Hahn et al. (1987), but are known to be biased low by -0.05 to -0.10 during dark winter conditions (Hahn et al. 1995).

In the Arctic, total cloud cover in July is close to observed, but there is too much low cloud cover (by about 0.10–0.15). In January, however, the total cloud cover is even higher (0.85–0.90), while the observations show about 0.50–0.60 (actually 0.60–0.70), with very little low cloud cover (about 0.20), whereas the model has a value about 0.80–0.90. (If one were to include the CE92 hypothesized wintertime ice crystal precipitation fraction of 0.50, along with their minimum cloud overlap assumption, the low cloud fraction would be

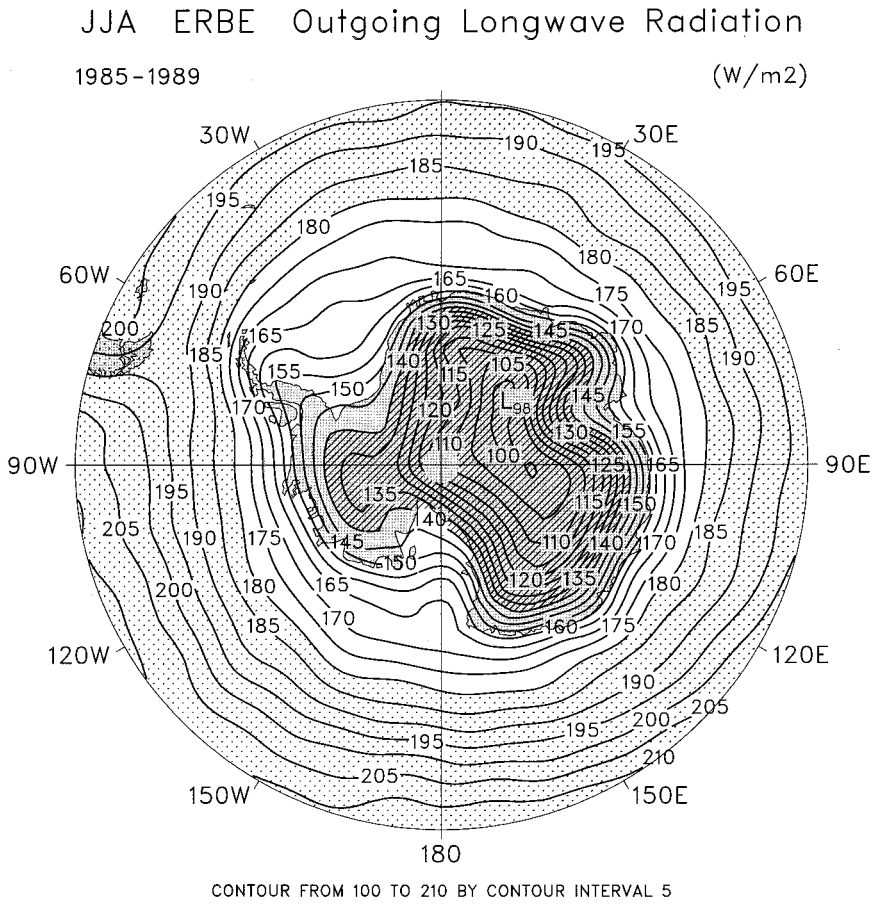

FIG. 10. (*Continued*)

0.70, closer to the model values.) Note that the simulated low cloud seasonal cycle is opposite to the observations, as found by Tzeng and Bromwich (1994) for CCM2. In the Antarctic a similar picture is seen: in local summer (January), CCM3 total cloud cover is slightly high (about 0.60 compared to 0.50 observed), whereas low cloud is significantly high (about 0.20 compared to 0.05 observed); in local winter (July), however, total cloud is extremely high (about 0.80–0.90 compared to 0.30 observed), again with too much low cloud (about 0.30–0.00 observed).

d. Cloud water path and particle size

CCM3 polar cloud simulation is illustrated by the mean vertical profiles in Fig. 14a for the Arctic summer and winter seasons, and in Fig. 14b for the Antarctic. The polar cap was restricted to 80° to the pole in this case to ensure a more homogeneous lower boundary. Shown are the mean ensemble air temperature and specific humidity profiles, reduced cloud cover (see below) and ice particle size (effective radius r_e) profiles, and cloud particle water paths CWP with phase. The lowest six CCM3 atmospheric layers have fractions of surface pressure of 0.990, 0.962, 0.920, 0.862, 0.789, and 0.701. Note that the CWPs show the actual model in-cloud *layer* paths, or $\mathrm{CWP}_k = \int_k \rho_l \, dz$ over the kth layer. Therefore, a 500-m summer stratus at 900 hPa would have a liquid water density ρ_l of about 0.13 g m^{-3}. Also, the area mean column CWP is cloud fraction weighted (as would be observed by satellite), and is $\Sigma_k A_{ck}\mathrm{CWP}_k$, the sum being over all vertical layers k. [Because of the reduction in the layer time-mean cloud fractions necessary to perform reasonable sensitivity calculations (see below), the column CWP values in Figs. 14a,b are less than those of CCM3. The polar cap values of CCM3 are 100.0 and 61.9 g m^{-2} (JJA and DJF, respectively) for the Arctic, and 45.3 and 33.3 g m^{-2} (DJF and JJA, respectively) for the Antarctic.]

For the Arctic in JJA season, the vertical cloud profile shows large amounts of low cloud and upper-level cloud (total cloud cover 0.79). The clouds are mostly water droplets of effective radius r_e of 10 μm in the lower troposphere, and ice in the upper troposphere of r_e from 20–30 μm, with total (reduced cloud fraction weighted) cloud water column of 54 g m^{-2}. DJF shows lower temperatures, vapor column, and total cloud water column, with nearly complete ice clouds. In the Antarctic,

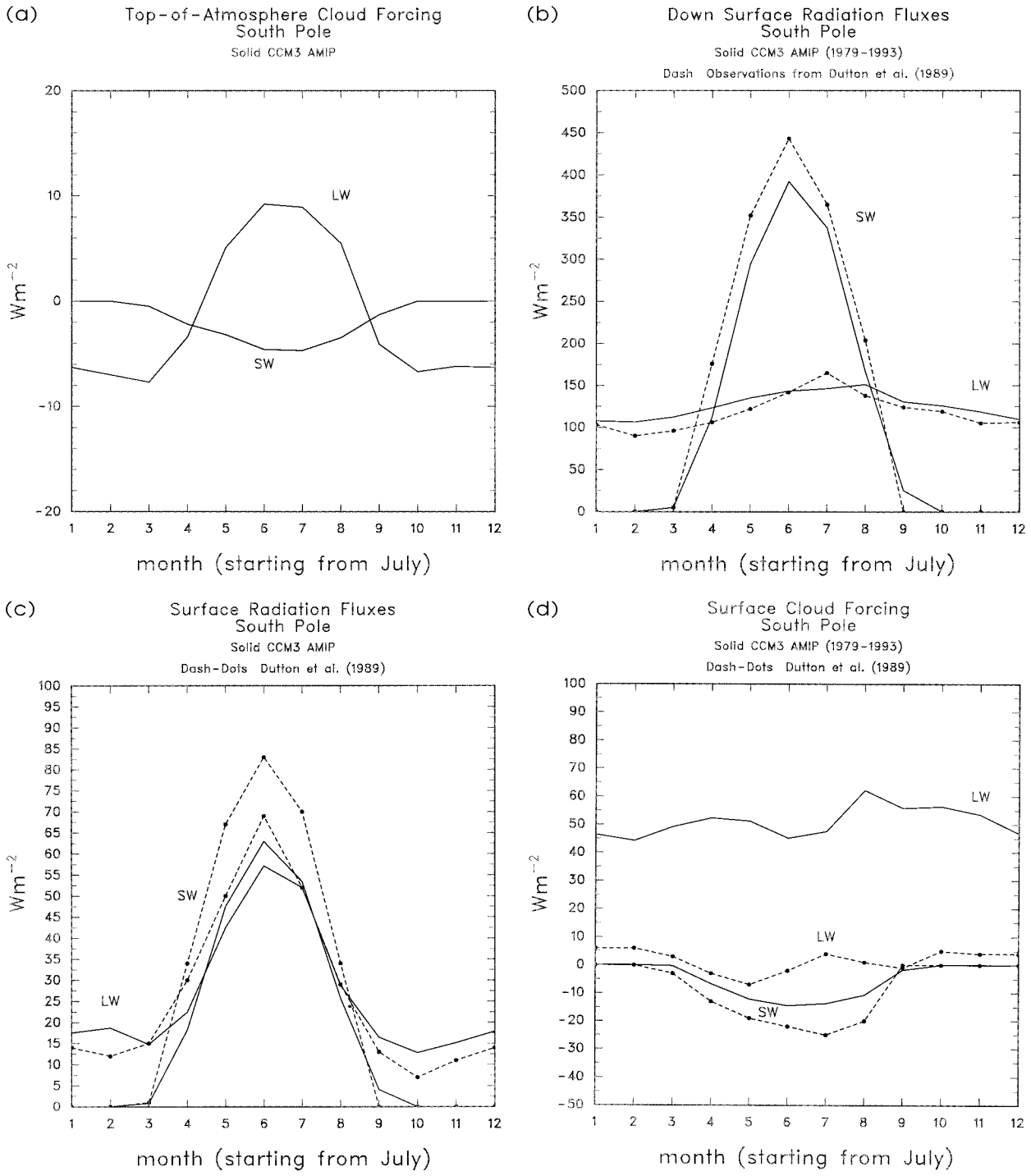

FIG. 11. Same as Fig. 6 except for the South Pole, using the observations from Dutton et al. (1989). Months are numbered with July as 1.

much lower temperatures result in very small vapor columns, cloud water columns (as low as 3.4 g m^{-2}), and nearly pure ice clouds of r_e from 10 to 30 μm.

For the Arctic, CE92 give winter cloud liquid water paths (LWPs) of 10 g m^{-2} and ice water paths (IWPs) around 50 g m^{-2}, whereas summer LWPs are around 60 g m^{-2} and IWPs about 5 g m^{-2}. Examination of Fig. 14a discloses that low-level winter cloud (800–950 hPa) would have LWP in the range 5–10 g m^{-2} and IWP around 70 g m^{-2}, and during summer the same thickness cloud would have LWP about 135 g m^{-2} and IWP (500–600 hPa) about 15–20 g m^{-2}. (We assume there are two

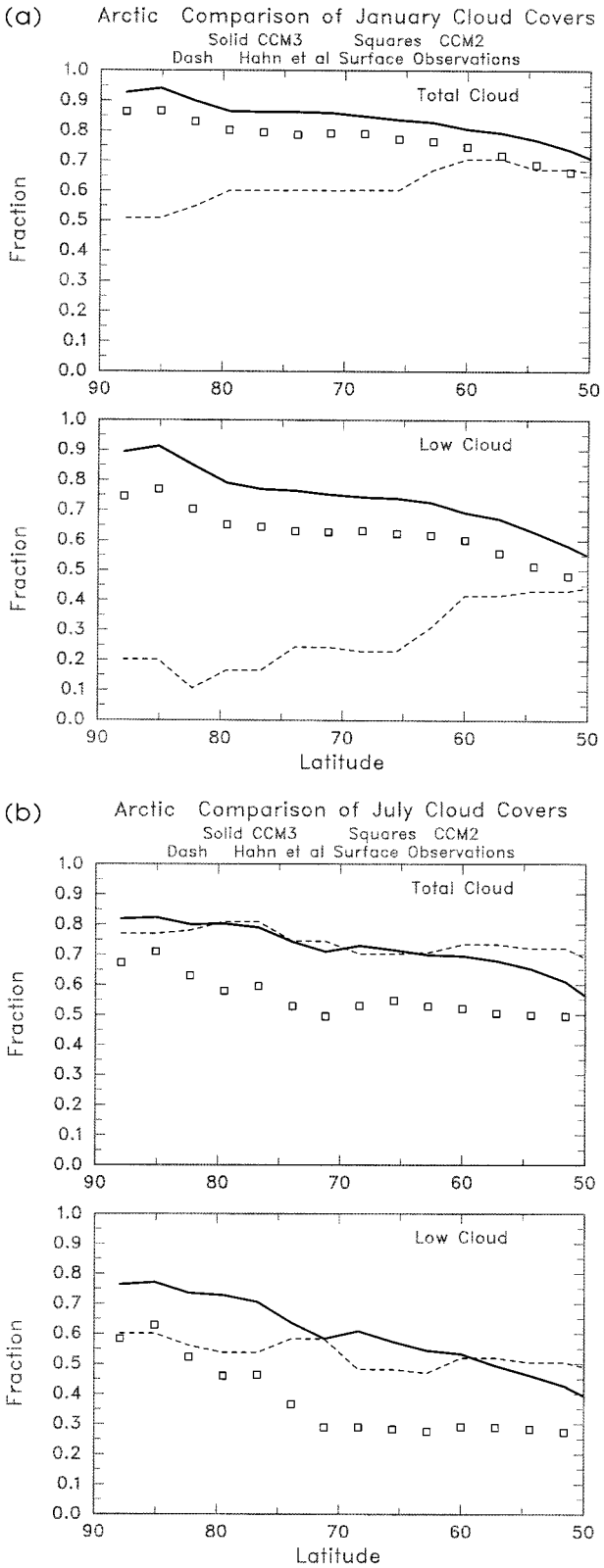

FIG. 12. Arctic (a) January and (b) July zonal mean 50°–90° latitude cloud covers (top panel total, lower panel low). Solid lines from the CCM3 AMIP integration (1979–93), dashes are surface observations from Hahn et al. (1987), and squares are from CCM2 (case 388, 20-yr ensemble mean).

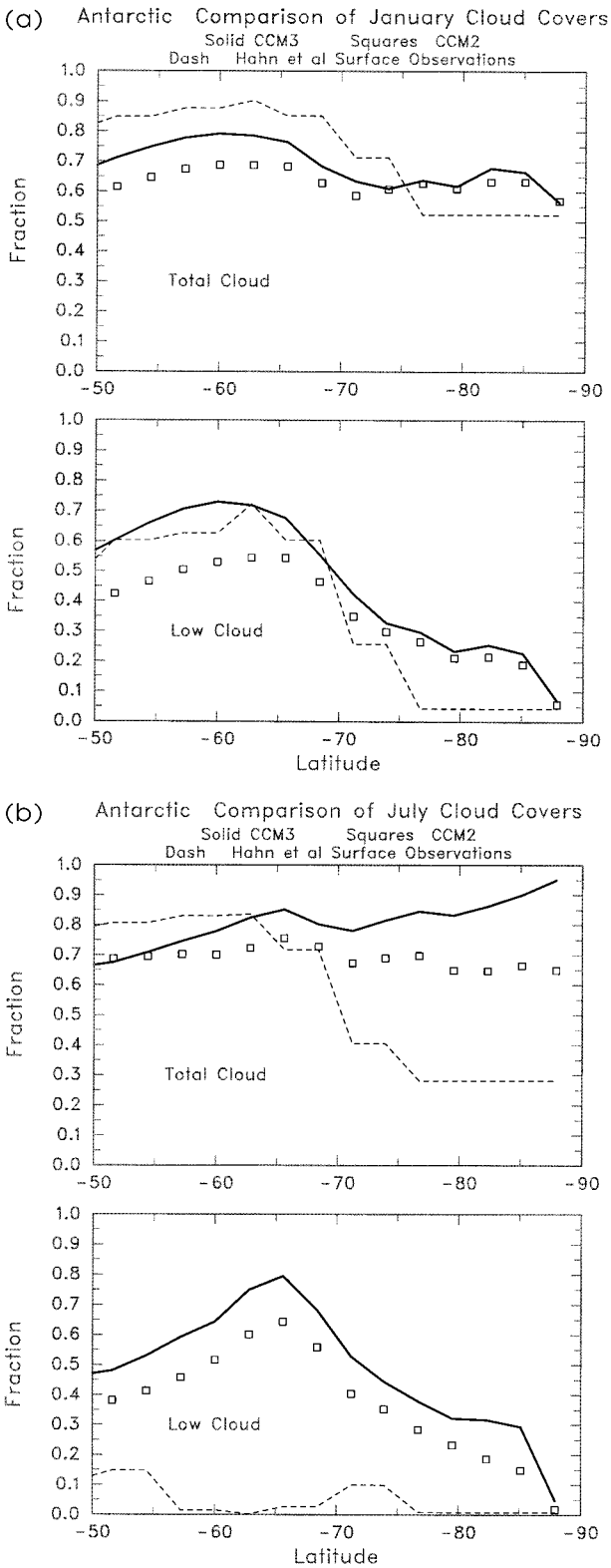

FIG. 13. Same as Fig. 12 except for the Antarctic.

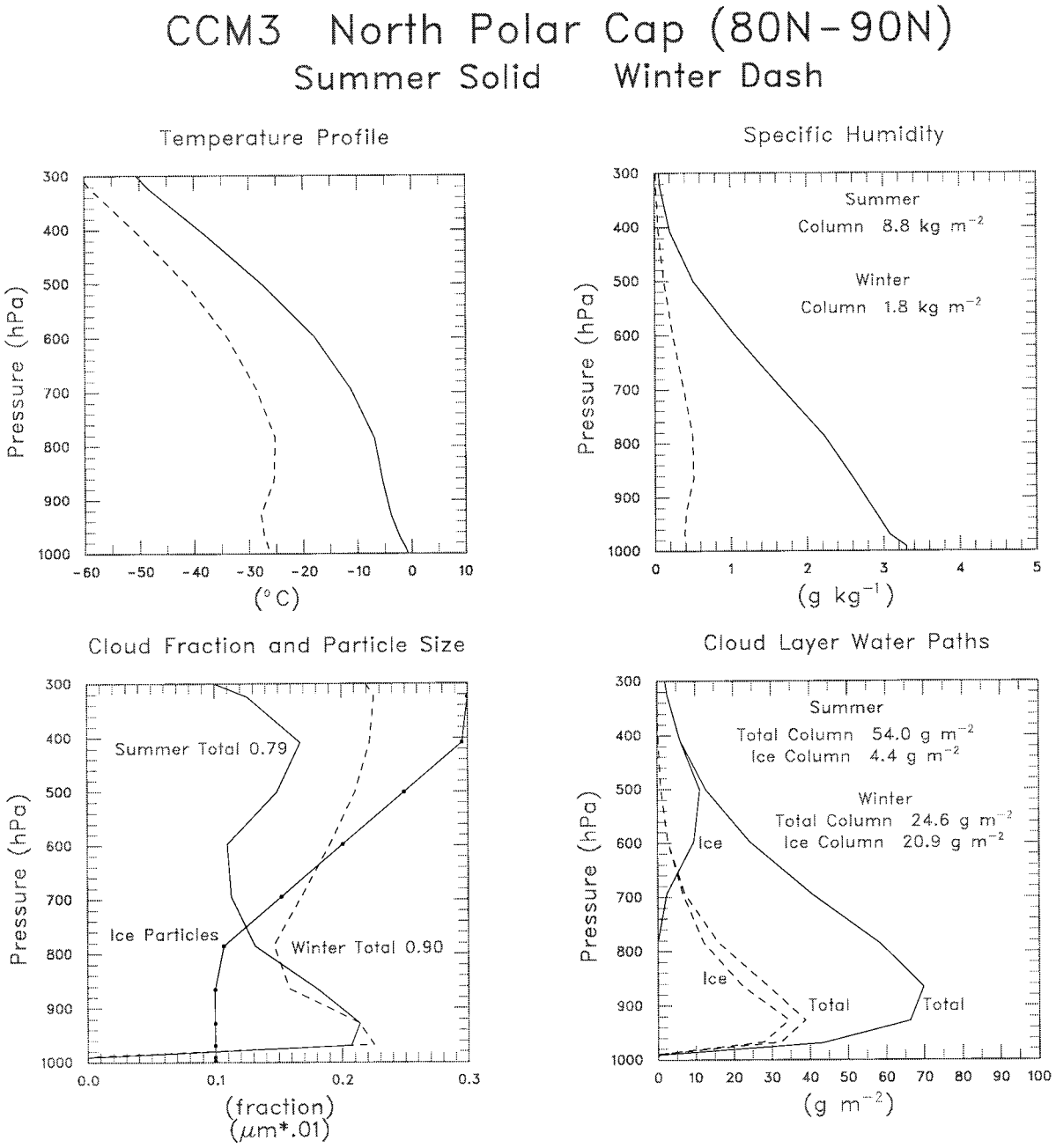

FIG. 14. Arctic (a) and Antarctic (b) polar cap (80°–90° lat) ensemble- and area-mean seasonal temperature, specific humidity, cloud fraction (reduced), cloud particle size, and cloud layer water path profiles from CCM3 AMIP integration (1979–93). Cloud fraction and 10^{-2} particle size (μm) are plotted on the same graph for conciseness, the latter as a solid-dot line, seasonally invariant. The total and ice CWP columns are cloud fraction weighted. Solid is summer, and dash is winter.

CCM3 cloud layers overlying one another, so that the total CWPs are the sums of those shown in Fig. 14a.) Thus, CCM3 Arctic clouds have too much summer CWP, by approximately a factor of 2. CE92 effective radii r_e for low-level liquid water clouds is 7.5 μm, whereas for lower-tropospheric ice clouds it is 40 μm and for upper-level cirrus clouds it is 14 μm. Thus, CCM3 summer Arctic stratus liquid r_e is slightly high (10 μm compared to 7.5 μm, although the CE92 value may be somewhat small), ice r_e is too small (10 μm compared to 40 μm) and too large (20–30 μm compared to 14 μm) for upper-level cirrus clouds (again, the CE92 value maybe too small). Too large a summer CWP implies large cloud shortwave optical depths, and hence polar clouds that are too reflective. The summer CWP and r_e values also result in low cloud emissivities of

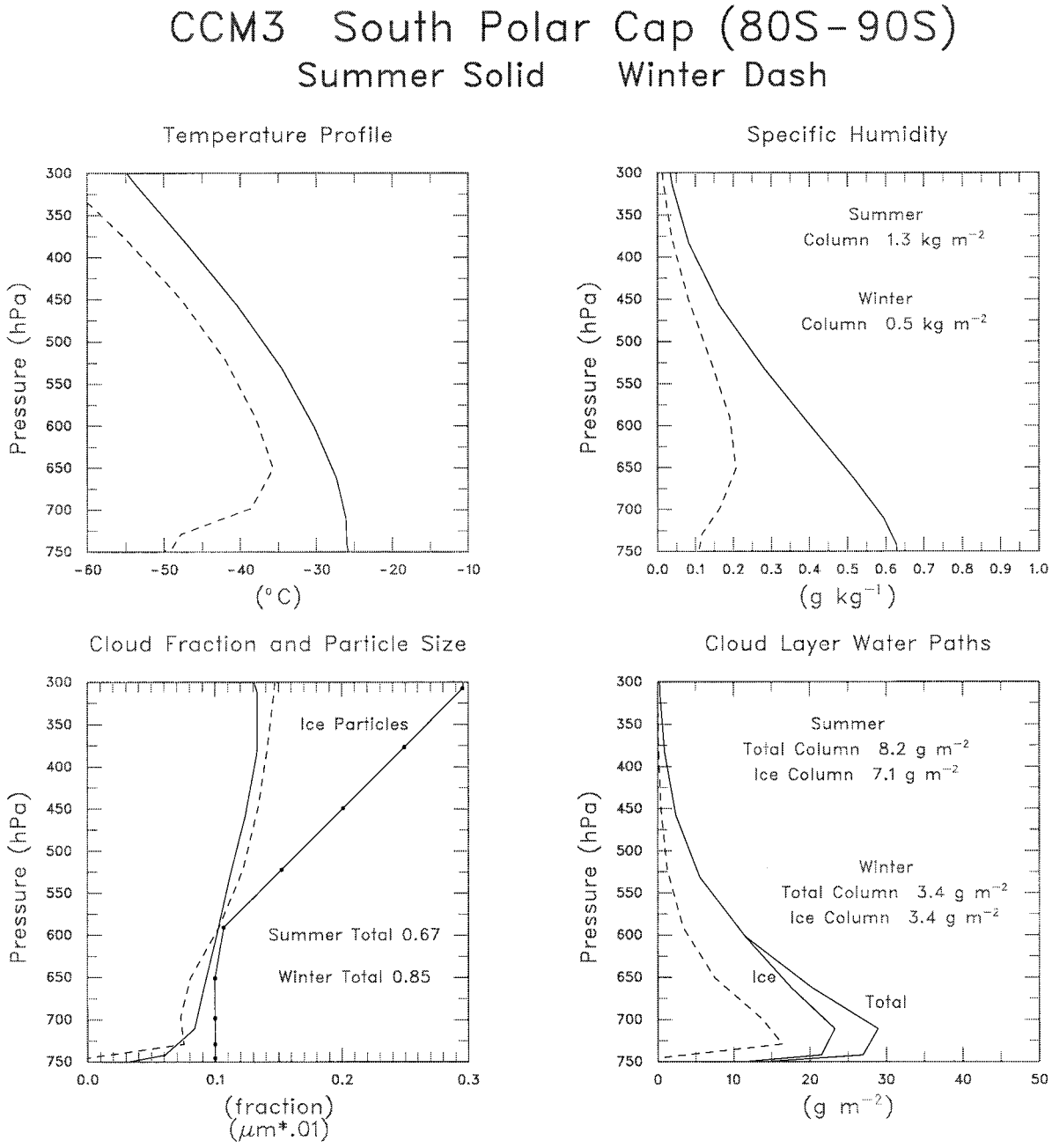

FIG. 14. (*Continued*)

1.0, and upper-level cirrus cloud values exceeding 0.95 (recall that cloud emissivity is $\epsilon_{cld} = 1 - e^{-1.66\kappa_{abs}CWP}$). During winter low cloud emissivities typically exceed 0.90. Thus, CCM3 Arctic clouds are too reflective in the shortwave and too emissive in the longwave.

Very little is known about the physical, microphysical, or radiative properties of Antarctic plateau clouds. The study of Stone (1993) probably represents one of the best available summaries. That study analyzed radiative properties of winter clouds at the South Pole based on a limited set of radiometersonde and coincident rawinsonde and surface sky cover observations during 1960–63. Several clear sky and overcast cases were selected. Winter meteorological conditions varied between steady downslope katabatic wind regimes associated with cold, generally clear skies and transient synoptic upslope disturbances originating from the Weddell Sea associated with relative warm (surface) overcast ice phase cloud systems above the surface inversion layer. Available but limited evidence suggest that transient winter clouds over much of the Antarctic plateau contain little or no liquid water, whereas summer clouds may

be of mixed phase. Mean effective broadband longwave emissivities were 0.6 ± 0.1, with associated optical depths ranging from 0.77 to 1.25. Based on theoretical models representing ice particles as equivalent spheres parameterized by their effective radii, cloud IWPs were found to range from 0.5 to 34 g m^{-2}, and effective radii varied from 4 to 16 μm. These cloud properties are comparable with in situ measurements made on midlatitude high-level cirrus clouds having similar mean temperatures (−5 to −40°C).

Examination of Fig. 14b for the South Pole cap mean CCM3 profiles of cloud properties shows that the cloud fractions for both winter and summer seasons are fairly uniform from 700 to 300 hPa. The winter cloud fractions continue to be large into the lower stratosphere, giving rise to the very different random overlap cloud fractions (0.85 versus 0.67). The mean winter CWPs for near complete coverage cloud in the range of 700–400 hPa would be approximately 10 g m^{-2}, well within the inferred range. The CCM3 effective radii ranging from 10 to 20 μm is somewhat larger than those inferred from data by Stone (1993). The resulting CCM3 winter cloud emissivity ranges from 0.81 for 10-μm effective radii to 0.56 for 20-μm effective radii; total cloud above 450 hPa having emissivities as low as 0.08. CCM3 summer mixed phase cloud emissivity for the 700–450-hPa cloud layer is 0.96. Thus, the CCM3 clouds appear to be somewhat too black in the longwave.

e. Longwave clear sky emission

As shown in Fig. 11d, there is a considerable discrepency between CCM3 surface LWCF and that estimated from the South Pole data of D89. As noted above, when clouds are present the downward LW is probably too high, but the bias in LWCF could also be due to the clear sky downward LW. Using the available LW output from CCM3, the clear sky downward LW can be estimated (note that the clear sky downward LW is calculated continuously by simply removing the clouds). The estimated clear sky downward LW is less than 70 W m^{-2} from April through September and has a minimum in August of 61 W m^{-2}. In contrast, the D89 data monthly minimum downward LW ranges from 70 to 90 W m^{-2} during winter, with an absolute minimum in August 1987 of 68 W m^{-2}. Given than the CCM3 clear sky downward LW is calculated at all times (therefore likely to have higher PW than for the true clear sky) and that the observed data generally range at least 10 W m^{-2} higher, there is likely to be a significant bias in CCM3 downward clear sky LW. Clear sky comparisons for both DJF and JJA between the longwave band model of Briegleb (1992) and CCM3 discloses a 1–2 W m^{-2} agreement in the TOA OLR but 6–7 W m^{-2} smaller CCM3 downward surface LW. Lubin and Harper (1996) estimate the bias to be between 20 and 25 W m^{-2}. Pinto et al. (1997) compared CCM2 LW calculations with observations (the low air temperatures in the comparisons imply the effects of trace gases and extra CO_2 bands in CCM3 are likely to be less than 2 W m^{-2}) and found low biases of 20 W m^{-2}. It is possible that for cold temperatures, strong low-level inversions, and low moisture amounts typical of polar climates, the water vapor rotation band emission is not being adequately simulated by the CCM3 LW radiation model (Curry et al. 1996; J. Kiehl 1997, personal communication).

f. Surface albedo

A large contributor to the low ASR over polar sea-ice-covered oceans is likely to be the high sea ice albedos. Broadband values of sea-ice albedo (without snow cover) are around 0.59, independent of temperature. A decrease in surface albedo of 0.15 due to the presence of melt ponds (which would result in a typical 0.44 summertime sea-ice albedo) would increase TOA ASR by an estimated (see below) 12 W m^{-2} (the surface absorption increases by 15 W m^{-2}), which eliminates much of the low ASR bias (see Figs. 3a,b). The snow–ice surface albedos over the Antarctic plateau are those of fresh snow (the underlying surface is a uniform glacial type away from the coast), having no soot, so that the albedos are very high (0.95 and 0.70 visible and near-IR, respectively). If these were reduced by 0.05, an increase in TOA ASR of 4 W m^{-2} would result, which reduces the negative bias somewhat (see Figs. 8a,b).

g. Radiative sensitivity calculations

The CCM3 polar cloud cover biases are similar in type and of the right sign to be consistent with the radiation budget biases. Too much cloud cover at all times of the year would reduce ASR in the local summer and increase the TOA OLR in local winter while decreasing it in local summer (because of the low-level temperature inversion in winter, excess low clouds can actually increase OLR). The CCM3 profiles shown in Figs. 14a,b can be used in conjunction with other data to perform sensitivity calculations with a column radiation model using the CCM3 radiation code. Cloud covers were reduced by vertically constant factors that produced the time-mean random overlap total cloud cover to within ±0.01 of the actual CCM3 mean. Time of year and day were adjusted to give TOA ASR to within ±5 W m^{-2} of actual CCM3 ensemble values, with the exception of the Antarctic polar cap. TOA OLR compared to within 10 W m^{-2} of actual CCM3 values. Sensitivity studies (over the central Arctic sea ice and Antarctic plateau regions) varying cloud cover and CWPs suggest only minimal improvements, generally less than 5 W m^{-2}, although correcting cloud covers to agree with the Hahn et al. (1987) data resulted in better agreement with the ERBE data. Increasing CWP by a factor of 10 between 300 and 700 hPa during winter conditions reduces Arctic OLR by 8 W m^{-2} and Ant-

arctic OLR by 1 W m^{-2}. As shown in Briegleb and Bromwich (1998), atmospheric polar temperatures are typically lower than the European Centre for Medium-Range Weather Forecasts analyses by 2°–3°C, especially in local summer. A uniform increase of 3°C for the entire column above the surface layer results in 9 W m^{-2} increase in TOA OLR in the Arctic JJA, and 6 W m^{-2} increase in the Antarctic DJF, removing the Arctic bias and substantially reducing the Antarctic (see Figs. 2 and 7).

It was noted above that the low CCM3 ASR extended from the Arctic Ocean into the surrounding polar land regions. Examination of the seasonal snow cover in Arctic land regions disclosed that very little snow cover exists for June and July, with only very small amounts on occasion in August. Thus, the low ASR is mostly due to clouds, and not to high surface albedo because of unmelted snow. In CCM3, the cloud effective radius over land for liquid droplets is assumed to be 5 μm, while it is 10 μm over ocean. For JJA conditions, a change in the effective radius from 5 μm to 10 μm would increase TOA ASR by about 45 W m^{-2}, whereas decreasing the CWP by a factor of 2 would increase it 23 W m^{-2}. Therefore, it is likely that biases in either cloud effective radius and/or CWP over summer polar land regions (Arctic) and summer coastal polar ocean regions (Antarctic) contribute to the low ASR.

Concerning extratropical CWP, we note the results of Hack et al. (1998), who compared CCM3 CWP with those derived from satellite (ocean only, nonprecipitating liquid water clouds). CCM3 has systematically lower zonal-mean ocean values (factor of 2 to 3) at low latitudes, but north and south of 40° lat, CCM3 values in general exceed the satellite values by 50% to 100%. These systematically higher polar ocean CCM3 CWP values are thus roughly consistent with the present results of low ASR over non-sea-ice polar surfaces. As just noted, a factor of 2 decrease in CWP over the summer poles would significantly reduce the negative bias in ASR.

4. Conclusions

We have presented the polar radiation budget simulation of uncoupled CCM3. We have shown how, in general, the CCM3 simulation has similar biases as that of CCM2, even though both versions of CCM are able to simulate many important polar radiation budget features. Several causes of polar radiation budget biases have been discussed. We now conclude by summarizing the suggested improvements that would significantly reduce these biases.

The most important cause of polar radiation budget biases is the cloud simulation. While cloud fraction is simulated fairly well, with the exception of winter low cloud, CWP is too high. The distinction between maritime and continental cloud particle size is too sharp along coastlines. Cloud particle phase is closely related to temperature, and thus is probably simulated fairly well. Ice particle sizes are somewhat small in the lower troposphere, but roughly the observed size for middle and high clouds. Prognostic cloud water schemes, such as those being developed for CCM (P. Rasch 1997, personal communication), may improve regional variability of cloud properties, but could still exhibit systematic biases. This subject requires further investigation.

A second important cause of polar radiation budget biases, especially in the surface radiation budget, is the low LW emission in the clear sky atmosphere. We have shown that clouds are compensating for this effect, especially during winter, where large low cloud covers and high CWP result in very emissive clouds. This clear sky LW bias is probably affecting the tropospheric fluxes and heating rates as well. Using line-by-line benchmark calculations and careful spectral analysis, it should be possible to correct the CCM3 water vapor rotation band absorption. This clear sky LW bias in CCM3 bears further attention.

A final important cause of polar radiation budget biases is the surface albedo simulation. Over sea ice there is the lack of melt ponds, and over continental glacial ice the surface albedos are systematically high. A fairly simple modification to sea-ice albedo that incorporates melt ponds would improve the simulation. For example, in the parameterization used in the CSM ice model (Bettge et al. 1996), ice albedo is decreased by 0.10 when surface melting is occuring. It should be possible to modify the glacial ice (covered with fresh snow) surface albedo prescription of the LSM (Bonan 1996) to produce more realistic surface albedos over the Antarctic plateau.

Last, we mention another possible bias in the CCM3 cloud radiative properties that would impact polar climate simulation. Recent studies (Zender et al. 1997 and references therein) indicate current radiation model clouds (including both CCM3 and CCM2) do not absorb sufficient shortwave radiation. The amount of enhanced shortwave absorption seems to increase with CWP, but the precise values are still being investigated. Yamanouchi and Charlock (1995), however, claim that no significant enhanced cloud absorption could be seen in their data for the South Pole. On the other hand, Herman and Curry (1984) reported measured values of cloud absorptivity that were systematically higher than those predicted, although they could not discount this discrepency as due to the uncertain effects of cloud geometry and inhomogeneity. Thus, whether enhanced cloud shortwave absorption exists in the polar regions is still an open question.

Kiehl et al. (1995) have discussed the impact of enhanced SW cloud absorption on the simulated climate of a developmental version of CCM3. They show that if the enhanced SW cloud absorption is a global phenonomenon with the magnitude of 20–25 W m^{-2}, then the potential impact on the summer polar atmosphere and surface is significant. For example, if polar clouds

absorb 10 W m^{-2} more and the surface 10 W m^{-2} more (due to better surface albedo prescription) then the TOA shortwave summer season bias in Table 1 would be removed. However, the import of enhanced shortwave absorption for climate modeling must await improved understanding of the responsible mechanism.

It should be noted that there continues to be a need for high quality polar radiation budget measurements for both clear and all sky conditions, especially at the surface. It is necessary to use results like those of CE92 due to lack of suitable observations, but it is preferable to have the direct observations themselves.

It is hoped that the improvements suggested here will result in a next-generation model with even better polar radiation budget simulation than that of CCM3. Such CCM3 simulation improvements cannot help but to improve coupled CSM simulations as well.

Acknowledgments. Charlie Zender of NCAR was helpful in providing the ERBE data. This research was supported in part by NSF Grant OPP-9224184 and by NASA Grant NAGW-2718, both to the second author. Comments by two anonymous reviewers resulted in many improvements to the paper.

REFERENCES

Barkstrom, B. R., and G. L. Smith, 1986: The earth radiation budget experiment: Science and implementation. *Rev. Geophys.,* **24,** 379–390.

Battisti, D. S., D. L. Williamson, and R. E. Moritz, 1992: Simulation of the Arctic climatology with the NCAR CCM2. Preprints, *Third Conf. on Polar Meteorology and Oceanography,* Portland, OR, Amer. Meteor. Soc., 130–136.

Bettge, T. W., J. W. Weatherly, W. M. Washington, D. Pollard, B. P. Briegleb, and W. G. Strand Jr., 1996: The NCAR CSM Sea Ice Model. NCAR/TN-425+STR, 25 pp. [Available from NCAR, Boulder, CO 80307.]

Bonan, G. B., 1996: A land surface model (LSM version 1.0) for ecological, hydrological, and atmospheric studies: Technical description of user's guide. NCAR/TN-417+STR, 150 pp. [Available from NCAR, Boulder, CO 80307.]

Boville, B. A., and P. R. Gent, 1998: The NCAR Climate System Model, version one. *J. Climate,* **11,** 1115–1130.

Briegleb, B. P., 1992: Longwave band model for thermal radiation in climate studies. *J. Geophys. Res.,* **97,** 11 475–11 485.

——, and D. H. Bromwich, 1998: Polar climate simulation of the NCAR CCM3. *J. Climate,* **11,** 1270–1286.

Bromwich, D. H., R.-Y. Tzeng, and T. R. Parish, 1994: Simulation of the modern Arctic climate by the NCAR CCM1. *J. Climate,* **7,** 1050–1069.

——, B. Chen, and R.-Y. Tzeng, 1995: Arctic and Antarctic precipitation simulations produced by the NCAR community climate models. *Ann. Glaciol.,* **21,** 117–122.

Curry, J. A., and E. E. Ebert, 1992: Annual cycle of radiation fluxes over the Arctic Ocean: Sensitivity to cloud optical properties. *J. Climate,* **5,** 1267–1280.

——, W. B. Rossow, D. Randall, and J. L. Schramm, 1996: Overview of Arctic cloud and radiation characteristics. *J. Climate,* **9,** 1731–1764.

Dutton, E. G., R. S. Stone, and J. L. Deluisi, 1989: South Pole surface radiation balance measurements April 1986 to February 1988. NOAA Data Rep. ERL ARL-17, 49 pp.

Gates, W. L., 1992: AMIP: The Atmospheric Model Intercomparison Project. *Bull. Amer. Meteor. Soc.,* **73,** 1962–1970.

Gloerson, P., W. J. Campbell, D. J. Cavalieri, J. C. Comiso, C. L. Parkinson, and H. J. Zwally, 1992: *Arctic and Antarctic Sea Ice, 1978–1987: Satellite Passive-Microwave Observations and Analysis.* NASA, 290 pp.

Hack, J. J., B. A. Boville, J. T. Kiehl, P. J. Rasch, and D. L. Williamson, 1994: Climate statistics from the National Center for Atmospheric Research Community Climate Model CCM2. *J. Geophys. Res.,* **99,** 20 785–20 813.

——, J. T. Kiehl, and J. W. Hurrell, 1998: The hydrologic and thermodynamic characteristics of the NCAR CCM3. *J. Climate,* **11,** 1179–1206.

Hahn, C. J., S. G. Warren, J. London, R. L. Jenne, and R. M. Chervin, 1987: Climatological data for clouds over the globe from surface observations. Rep. NDP-026, 57 pp. [Available from Carbon Dioxide Information Center, Oak Ridge, TN 37831-6050.]

——, ——, and ——, 1995: The effect of moonlight on observation of cloud cover at night, and application to cloud climatology. *J. Climate,* **8,** 1429–1446.

Harrison, E. F., P. Minnis, B. R. Barkstrom, V. Ramanathan, R. D. Cess, and G. G. Gibson, 1990: Seasonal variation of cloud radiative forcing derived from the Earth Radiation Budget Experiment. *J. Geophys. Res.,* **95,** 18 687–18 703.

Herman, G. F., and J. A. Curry, 1984: Observational and theoretical studies of solar radiation in Arctic stratus clouds. *J. Climate Appl. Meteor.,* **23,** 5–24.

Hurrell, J. W., J. J. Hack, B. A. Boville, D. L. Williamson, and J. T. Kiehl, 1998: The dynamical simulation of the NCAR Community Climate Model, version 3 (CCM3). *J. Climate,* **11,** 1207–1236.

Kiehl, J. T., J. J. Hack, and B. P. Briegleb, 1994: The simulated earth radiation budget of the National Center for Atmospheric Research Community Climate Model CCM2 and comparisons with the Earth Radiation Budget Experiment. *J. Geophys. Res.,* **99,** 20 815–20 827.

——, ——, M. H. Zhang, and R. D. Cess, 1995: Sensitivity of a GCM climate to enhanced shortwave cloud absorption. *J. Climate,* **8,** 2200–2212.

——, ——, G. B. Bonan, B. A. Boville, B. P. Briegleb, D. L. Williamson, and P. J. Rasch, 1996: Description of the NCAR Community Climate Model (CCM3). NCAR/TN-420+STR, 152 pp. [Available from NCAR, Boulder, CO 80307.]

——, ——, ——, ——, D. L. Williamson, and P. J. Rasch, 1998a: The National Center for Atmospheric Research Community Climate Model: CCM3. *J. Climate,* **11,** 1131–1149.

——, ——, and J. W. Hurrell, 1998b: The energy budget of the NCAR Community Climate Model: CCM3. *J. Climate,* **11,** 1151–1178.

Li, Z., and H. G. Leighton, 1991: Scene identification and its effect on cloud radiative forcing in the Arctic. *J. Geophys. Res.,* **96,** 9175–9188.

——, and ——, 1993: Global climatologies of solar radiation budgets at the surface and in the atmosphere from 5 years of ERBE data. *J. Geophys. Res.,* **98,** 4919–4930.

——, ——, K. Masuda, and T. Takashima, 1993a: Estimation of SW flux absorbed at the surface from TOA reflected flux. *J. Climate,* **6,** 317–330.

——, ——, and R. D. Cess, 1993b: Surface net solar radiation estimated from satellite measurements: Comparisons with tower observations. *J. Climate,* **6,** 1764–1772.

Lubin, D., and D. A. Harper, 1996: Cloud radiative properties over the South Pole from AVHRR infrared data. *J. Climate,* **9,** 3405–3418.

——, B. Chen, D. H. Bromwich, R. C. J. Somerville, W.-H. Lee, and K. M. Hines, 1998: The impact of Antarctic cloud radiative properties on a GCM climate simulation. *J. Climate,* **11,** 447–462.

Nemesure, S., R. D. Cess, E. G. Dutton, J. L. Deluisi, Z. Li, and H. G. Leighton, 1994: Impact of clouds on the shortwave ra-

diation budget of the surface-atmosphere system for snow-covered surfaces. *J. Climate,* **7,** 579–585.

Pinto, J. O., J. A. Curry, and C. W. Fairall, 1997: Radiative characteristics of the Arctic atmosphere during spring as inferred from ground-based measurements. *J. Geophys. Res.,* **102,** 6941–6952.

Reynolds, R. W., and D. C. Marciso, 1993: An improved real-time global sea surface temperature analysis. *J. Climate,* **6,** 114–119.

Schweiger, A. J., and J. R. Key, 1994: Arctic ocean radiative fluxes and cloud forcing estimated from the ISCCP C2 cloud dataset, 1983–1990. *J. Appl. Meteor.,* **33,** 948–963.

Stone, R. S., 1993: Properties of austral winter clouds derived from radiometric profiles at the South Pole. *J. Geophys. Res.,* **98,** 12 961–12 971.

Tzeng, R.-Y., and D. H. Bromwich, 1994: NCAR CCM2 simulations of present-day Arctic climate. Preprints, *Sixth Conf. on Climate Variations,* Nashville, TN, Amer. Meteor. Soc., 197–201.

——, ——, and T. R. Parish, 1993: Present-day Antarctic climatology of the NCAR Community Climate Model version 1. *J. Climate,* **6,** 205–226.

——, ——, ——, and B. Chen, 1994: NCAR CCM2 simulation of the modern Antarctic climate. *J. Geophys. Res.,* **99,** 23 131–23 148.

Wild, M., A. Ohmura, H. Gilgen, and E. Roeckner, 1995: Validation of general circulation model radiative fluxes using surface observations. *J. Climate,* **8,** 1309–1324.

Williamson, D. L., D. H. Bromwich, and R.-Y. Tzeng, 1996: Further discussion on simulation of the modern Arctic climate by the NCAR CCM1. *J. Climate,* **9,** 1669–1672.

Yamanouchi, T., and T. P. Charlock, 1995: Comparison of radiation budget at the TOA and surface in the Antarctic from ERBE and ground surface measurements. *J. Climate,* **8,** 3109–3120.

Zender, C. S., B. Bush, S. K. Pope, A. Bucholtz, W. D. Collins, J. T. Kiehl, F. P. J. Valero, and J. Vitko Jr., 1997: Atmospheric absorption during the Atmospheric Radiation Measurement (ARM) Enhanced Shortwave Experiment (ARESE). *J. Geophys. Res.,* **102,** 29 901–29 915.